NAVAL POSTGRADUATE SCHOOL
Monterey, California

DTIC QUALITY INSPECTED 2

THESIS

SIMULATIONS OF THE LANL
1 KW REGENERATIVE AMPLIFIER FEL

by

Mark D. Kesselring

December, 1997

Thesis Advisor:	William B. Colson
Second Reader:	Robert L. Armstead

Approved for public release; distribution is unlimited.

19980424 035

REPORT DOCUMENTATION PAGE

Form Approved
OMB No. 0704-0188

Public reporting burden for this collection of information is estimated to average 1 hour per response, including the time for reviewing instruction, searching existing data sources, gathering and maintaining the data needed, and completing and reviewing the collection of information. Send comments regarding this burden estimate or any other aspect of this collection of information, including suggestions for reducing this burden, to Washington headquarters Services, Directorate for Information Operations and Reports, 1215 Jefferson Davis Highway, Suite 1204, Arlington, VA 22202-4302, and to the Office of Management and Budget, Paperwork Reduction Project (0704-0188) Washington DC 20503.

1. AGENCY USE ONLY *(Leave blank)*	2. REPORT DATE	3. REPORT TYPE AND DATES COVERED
	December 1997	Master's Thesis

4. TITLE AND SUBTITLE
SIMULATIONS OF THE LANL 1 KW REGENERATIVE AMPLIFIER FEL

5. FUNDING NUMBERS

6. AUTHOR(S)
Kesselring, Mark D.

7. PERFORMING ORGANIZATION NAME(S) AND ADDRESS(ES)
Naval Postgraduate School
Monterey, CA 93943-5000

8. PERFORMING ORGANIZATION REPORT NUMBER

9. SPONSORING / MONITORING AGENCY NAME(S) AND ADDRESS(ES)

10. SPONSORING / MONITORING AGENCY REPORT NUMBER

11. SUPPLEMENTARY NOTES
The views expressed in this thesis are those of the author and do not reflect the official policy or position of the Department of Defense or the U.S. Government.

12a. DISTRIBUTION / AVAILABILITY STATEMENT
Approved for public release; distribution is unlimited.

12b. DISTRIBUTION CODE

13. ABSTRACT *(maximum 200 words)*

The development of a high average power FEL for military applications would represent a significant improvement in missile defense, especially shipboard self-defense. The LANL regenerative amplifier FEL (RAFEL) is designed to produce an average output power of 1 kW. This FEL represents a significant increase in average power demonstrated in an FEL and also provides a test of the concept of combining the FEL oscillator and amplifier designs. Simulations were performed to better understand the physics behind the LANL RAFEL operation.

Simulations study the transverse effects due to optical guiding by the intense electron beam and feedback. These simulations are applied to optimizing the undulator taper rate, feedback optimization, and initial phase velocity. Additional simulations study the longitudinal effects due to short electron pulses and optical pulse development over multiple passes. Finally, simulations of the RAFEL design using an ideal beam expand on understanding of the design's basic characteristics and limitations.

14. SUBJECT TERMS	15. NUMBER OF PAGES
FEL, Free Electron Laser, Laser, amplifier, oscillator, RAFEL, LANL	70
	16. PRICE CODE

17. SECURITY CLASSIFICATION OF REPORT	18. SECURITY CLASSIFICATION OF THIS PAGE	19. SECURITY CLASSIFICATION OF ABSTRACT	20. LIMITATION OF ABSTRACT
Unclassified	Unclassified	Unclassified	UL

NSN 7540-01-280-5500

Standard Form 298 (Rev. 2-89)
Prescribed by ANSI Std. 239-18

Approved for public release; distribution is unlimited

SIMULATIONS OF THE LANL 1 KW REGENERATIVE AMPLIFIER FEL

Mark D. Kesselring
Lieutenant, United States Navy
B.S., University of Colorado, Boulder, 1991

Submitted in partial fulfillment of the
requirements for the degree of

MASTER OF SCIENCE IN APPLIED PHYSICS

from the

NAVAL POSTGRADUATE SCHOOL
December 1997

Author: _____
Mark D. Kesselring

Approved by: _____
William B. Colson, Thesis Advisor

_____
Robert L. Armstead, Second Reader

_____
William B. Maier II, Chairman
Department of Physics

ABSTRACT

The development of a high average power FEL for military applications would represent a significant improvement in missile defense, especially shipboard self-defense. The LANL regenerative amplifier FEL (RAFEL) is designed to produce an average output power of 1 kW. This FEL represents a significant increase in average power demonstrated in an FEL and also provides a test of the concept of combining the FEL oscillator and amplifier designs. Simulations were performed to better understand the physics behind the LANL RAFEL operation.

Simulations study the transverse effects due to optical guiding by the intense electron beam and feedback. These simulations are applied to optimizing the undulator taper rate, feedback optimization, and initial phase velocity. Additional simulations study the longitudinal effects due to short electron pulses and optical pulse development over multiple passes. Finally, simulations of the RAFEL design using an ideal beam expand on understanding of the design's basic characteristics and limitations.

TABLE OF CONTENTS

ACKNOWLEDGMENT

The author is grateful to Professor Bill Colson, Professor Bob Armstead, and Dr. Robert Wong for their invaluable assistance and guidance throughout this project.

The author would also like to acknowledge the kindness and support of his loving wife Mika and their daughter Irena.

I. INTRODUCTION

A. INADEQUATE SHIP SELF-DEFENSE

The world we live in today is very complex and dangerous. At the beginning of the decade the United States had a single adversary and a well defined mission. Since the end of the "cold war" both this mission and this single adversary have gone away. On the surface this sounds like a good thing. In reality it is a very unstable situation. The tight control over nuclear weapons and missiles is no longer there. Consequently missile technology and nuclear weapons are available to any country or organization with enough money to buy them. Additionally, the focus of the United States Navy is no longer that of a "blue water" navy. We no longer plan to fight large naval battles in the middle of the ocean. The mission of late has been in the littoral environment. Operating our ships near land puts them in the line of fire of even the crudest missiles. The close proximity to fire and proliferation of missile and nuclear technology make a good case for enhancing ship self-defense.

Possibly more significant is the rate at which offensive missile technology continues to advance. Current approaches at ship self-defense are unable to keep up. The Close-In Weapons System (CIWS) is ineffective. The system just can not hit the newer missiles at sufficiently large ranges to protect the ship from debris. If the CIWS hits the missile at close range, the fragments would continue onward to inflict serious damage on the ship. The defensive missile concept has serious drawbacks. In this era of significant

cutbacks the excessive cost of each missile is unacceptable. In order to effectively defeat newer offensive missiles, new defensive missile cost is skyrocketing. This brings us to the inherent flaw in the defensive missile concept. If technology is invented for the defensive missile to improve its design over the offensive missile that technology is available for the offensive missile. This is unacceptable because the defensive missile has to be significantly better than the offensive missile to defeat it. A new weapon is needed as an alternative; this weapon is a "speed of light" weapon.

This type of weapon would have speed of light response and could engage a target on the horizon. This is significant considering the prevalence of nuclear weapons we are facing. Destroying one on the horizon is infinitely more desirable than a few hundred yards one might get with CIWS. The concept of using a directed energy weapon, or a laser, for defense is not new. In fact, "technologies already exist and deployable HEL (High Energy Laser) weapons systems are just beyond the horizon, whether the United States Navy is pushing or not." [1]

B. THE FREE ELECTRON LASER (FEL) SOLUTION

There are many directed energy and laser technologies developed and being developed. In fact, the MIRACL laser, a chemical laser, has been tested in White Sands, NM to shoot down various missiles. A few significant obstacles are power consumption, availability of space, and propagation through the atmosphere.

The power consumption problem depends on the choice of high energy weapon. For instance, a chemical laser would have to carry significant amounts of chemical reactant while a free electron laser (FEL) would need about 10 MW of power to operate continuously [2]. Substantially less power is nedded for operation in a limited engagement. This leads to the next major shipboard problem of where to put such a system on a ship. There just is not enough room on current ships, such as the DDG 51, to add another weapon system. However, ref. [2] describes how an FEL and its prime power could be retrofit on a DDG 51. It could fit into the space of a 32 cell Vertical Launch System (VLS) weapon. When looking to minimize space and power consumption it is important to look at an HEL systems efficiency. The FEL may be able to achieve 10% system efficiency. However, a crucial problem remains, atmospheric propagation.

The MIRACL laser was tested over a desert area. There are only small wavelength windows where a high energy laser beam can be successfully propagated over long distances. While it is possible to find a laser that will work at these wavelengths, it is not possible to adjust these lasers to variable weather patterns around the globe. The FEL is tunable and designable in wavelength. Once it is designed for a certain wavelength, it can be adjusted to another wavelength for optimum propagation with relative ease. Primarily for this reason the FEL is ideal for development as a shipboard self-defense weapon system.

This thesis discusses a relatively new design for the FEL. In the past, FEL designs were either oscillators, which relied on many passes to achieve gain, or amplifiers, which have very high gain in a single pass. Los Alamos National Laboratory (LANL) has built

an FEL which combines both these designs. The LANL design is called a regenerative amplifier FEL (RAFEL) and relies on only a few passes to achieve high power.

After a review of basic FEL theory, a detailed description of the RAFEL will be presented. The contribution of this thesis is to present results of simulations of the RAFEL to better understand the physics behind its operation. By simulating the diffractive effects inside the undulator, the optimum taper rate and feedback where obtained. These were optimized to achieve maximum operating efficiency. Using the same simulation the initial phase velocity was varied to explore possible wavelength variations. Finally, the pulse evolution along the undulator was simulated in order to understand the effects of short pulses. A better understanding of the physics of the FEL interaction can lead to more compact and more efficient FEL systems in the future.

II. FREE ELECTRON LASER PHYSICS

A. INTRODUCTION

The basic mechanism behind the free electron laser (FEL) is that electrons will radiate energy coherently when bunched at optical wavelengths. The FEL makes use of this process by bending a high energy beam of electrons back and forth causing them to radiate in an undulator.

The main components of an FEL are an accelerator, an undulator, and for the oscillator design an optical resonator. There are also focusing elements and the source of electrons, an electron gun. The basic configuration is shown in Figure 1.

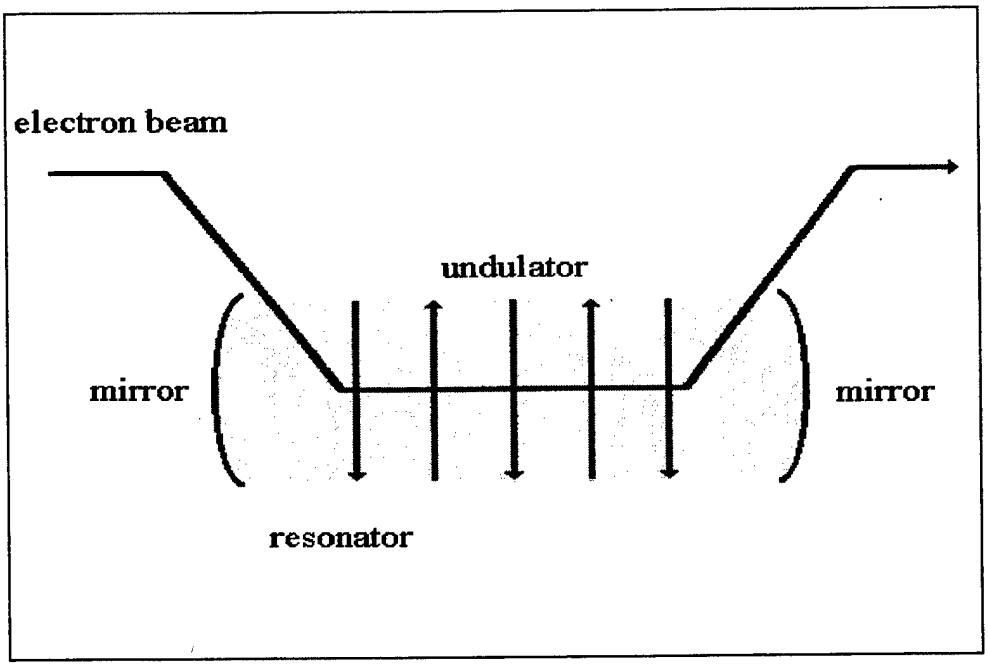

Figure 1. Basic components of an FEL.

A beam of electrons is injected into the accelerator which speeds them to relativistic velocities. These relativistic electrons are focused through an undulator. The undulator consists of static magnetic fields alternating in direction, normally from fixed magnets, which bend the electron beam. The beam of electrons then radiates forward in the direction of motion of the electrons. In the oscillator configuration this optical power is stored in the resonator cavity and will build over several passes until saturation is reached. Saturation is marked by decreased gain and by the field amplitude reaching its maximum value. In the amplifier configuration, there is much higher gain and the optical field grows significantly in a single pass. The physics of the electron motion in the undulator is governed by classical electromagnetic theory as described in the next section.

B. PENDULUM EQUATION

To understand the forces in the undulator, the transfer of momentum and energy between a free electron and an electromagnetic wave must be evaluated. A helical magnetic field in the undulator is assumed for the following calculations. The forces acting on the electrons in the undulator are governed by the following equations:

$$\frac{d}{dt}\left(\gamma\vec{\beta}\right) = -\frac{e}{mc}\left[\vec{E} + \vec{\beta}\times\vec{B}\right] \quad , \tag{1}$$

$$\frac{d\gamma}{dt} = -\frac{e}{mc}\left[\vec{\beta}\cdot\vec{E}\right] \quad , \tag{2}$$

$$\gamma = \frac{1}{\sqrt{1-\vec{\beta}\cdot\vec{\beta}}} \quad . \tag{3}$$

The optical electric field is $\vec{E}_s = E[\cos\Psi, -\sin\Psi, 0]$ and the optical magnetic field is $\vec{B}_s = E[\sin\Psi, \cos\Psi, 0]$, where $\Psi = kz - \omega t + \phi$. The optical wavenumber is $k = \omega / c = 2\pi / \lambda$ and ϕ is the optical phase. The velocity of the electron is given by $c\vec{\beta}$. The undulator field in a helical undulator is $\vec{B} = B[\cos(k_0 z), \sin(k_0 z), 0]$, where B is the magnitude of the undulator magnetic field and $k_0 = 2\pi / \lambda_0$ is the undulator wave number [3]. Equations (1), (2), and (3) describe the conservation of momentum, energy transfer and define the Lorentz factor, respectively. Insert the optical and undulator fields into (1) and integrate to get $\vec{\beta}_\perp = -K(\cos k_0 z, \sin k_0 z, 0) / \gamma$ where $K = eB / k_0 mc^2$ is called the "undulator parameter". Taking this result and inserting into (2) yields

$$\dot{\gamma} = \frac{eKE}{\gamma mc}\cos(\zeta + \phi) \quad , \tag{4}$$

where $\zeta = (k + k_0)z - \omega t$ and $\dot{\gamma} = d\gamma / dt$. In order to continue in the development of the pendulum equation, it is useful to understand the FEL resonance condition.

Think of the electron and photon racing along the undulator. In Figure 2, the photon is represented by a grey wavelength and the black dot is the electron. One undulator wavelength is shown as a dark curve. Resonance occurs when one wavelength of light passes over an electron while the electron travels through one undulator wavelength. Recall that the electron is traveling at a speed $\beta_z c$ where c is the speed of light. The condition for resonance is given by

$$\lambda = \lambda_0 \frac{1 + K^2}{2\gamma^2} \quad , \tag{5}$$

where λ is the light wavelength and λ_0 is the undulator wavelength.

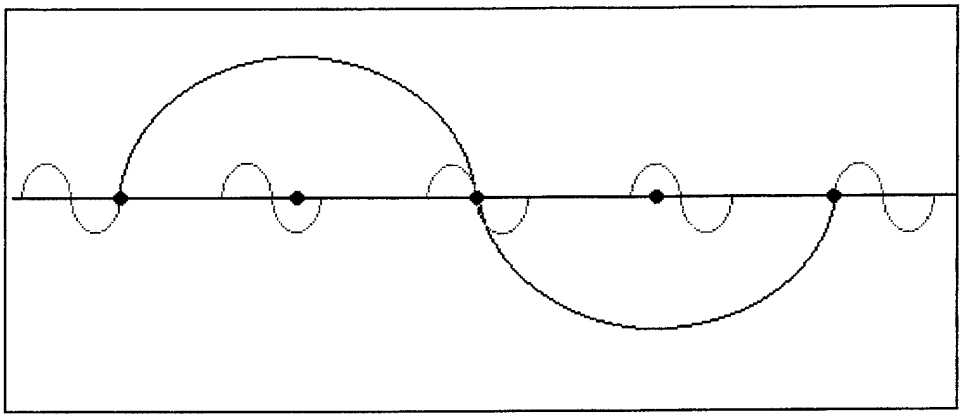

Figure 2. Electron-Photon race.

Inserting $\vec{\beta}_\perp$ into (3) gives a relationship between $\dot{\gamma}$ and $\dot{\beta}_z$. This can then be combined with (5) to rewrite (4) in the familiar form of the pendulum equation,

$$\ddot{\zeta} = \frac{2k_0 eKE}{\gamma^2 m}\cos(\zeta + \phi) \quad . \tag{6}$$

This equation describes the electron phase dynamics as they evolve through the undulator.

The amount of time the average electron spends in the undulator is given by the length of the undulator divided by the average electron velocity. Since bunching of electrons occurs over a length significantly smaller than the undulator length this time is about the same for all electrons. In order to convert to dimensionless units, a dimensionless time $\tau = \beta ct / L \approx ct / L$ will be introduced, where L is the length of the undulator and βc is the average electron velocity. According to this definition $0 \le \tau \le 1$ along the entire undulator. Substitute $dt = Ld\tau / c$ into (6) for the final form of the pendulum equation

$$\overset{oo}{\zeta} = |a|\cos(\zeta + \phi) \quad , \tag{7}$$

where $\overset{oo}{\zeta} = d^2\zeta / d\tau^2$ and $|a| = 4\pi NeKLE / \gamma^2 mc^2$ is the magnitude of the dimensionless optical field. This equation governs the motion of the electrons in phase space. In order to arrive at this final solution it was assumed that the electrons are relativistic and that the change in the electron energy is relatively small along the undulator [3]. Having developed the equation describing the electron trajectory in the undulator the physics of the optical wave must be understood.

C. WAVE EQUATION

In the FEL, the light wave is amplified by stimulated emission. An equation describing the light wave dynamics can be developed starting from Maxwell's wave equation,

$$\left(\vec{\nabla}^2 - \frac{1}{c^2}\frac{\partial^2}{\partial t^2}\right)\vec{A}(\vec{x},t) = -\frac{4\pi}{c}\vec{J}_\perp(\vec{x},t) \quad . \tag{8}$$

The vector potential is $\vec{A}(\vec{x},t) = \vec{E}(\vec{x},t)(\sin\Psi, \cos\Psi, 0)/k$ and $\vec{J}_\perp(\vec{x},t)$ is the total beam current. Define the complex electric field $\boldsymbol{\mathcal{E}}(\vec{x},t) = E(\vec{x},t)e^{i\phi(\vec{x},t)}$, and rewrite the vector potential $\vec{A}(\vec{x},t) = \boldsymbol{\mathcal{E}}(\vec{x},t)\hat{e}e^{i\alpha}/k$ where $\alpha = kz - \omega t$ and $\hat{e} = (-i,0,0)$. Assume that both E and ϕ are slowly varying in z and t, and complete the left side of (8). This allows the wave equation to be written as

$$\left[\frac{1}{2}\vec{\nabla}^2 + ik\left(\pm\frac{\partial}{\partial z} + \frac{1}{c}\frac{\partial}{\partial t}\right)\right]\boldsymbol{\mathcal{E}}(\vec{x},t) = -\frac{\pi k}{c}\vec{J}_\perp \cdot \hat{e}^* e^{-i\alpha} \quad . \tag{9}$$

The current is the sum over all single particle currents,

$$\vec{J}_\perp = -ec\sum_i\left(\vec{\beta}_\perp \delta^{(3)}\left(\vec{x} - \vec{r}_i(t)\right)\right) \quad . \tag{10}$$

Identify $\zeta = k_0 z + \alpha = (k_0 + k)z - \omega t$ and simplify the sum by using the weight factor $\rho(\vec{x},t)$ = electron density at $\vec{x}$. Then assuming the positive solution of ζ the wave equation becomes

$$\left(\frac{1}{2}\vec{\nabla}^2 + ik\left(\frac{\partial}{\partial z} + \frac{1}{c}\frac{\partial}{\partial t}\right)\right)\mathcal{E}(\vec{x},t) = -2\pi ieKk\rho(\vec{x},t)\left\langle\frac{e^{i\zeta}}{\gamma}\right\rangle_{(\vec{x},t)} \quad , \tag{11}$$

where $\langle\ \rangle_{(\vec{x},t)}$ is the average over a sample including a number of electrons in one periodic section of phase space located at position $(\vec{x},t)$. In (11), $\mathcal{E}(\vec{x},t)$ is an envelope of the optical field driven by the current density $\rho(\vec{x},t)$. The term $\langle\ \rangle_{(\vec{x},t)}$ defines the degree of electron bunching in the volume $(\vec{x},t)$.

Equation (11) must be made dimensionless to correspond to the development of (7). In addition to the dimensionless time $\tau = tc/L$, the coordinate transformation $\tilde{z} = z - ct$ makes the frame of reference that of the electron beam. Applying the chain rule and after some algebraic manipulation [4], the wave equation can be written as

$$\left(-\frac{iL}{2k}\vec{\nabla}^2 + \frac{\partial}{\partial\tau}\right)a(x,y,\tilde{z},\tau) = -\left\langle je^{-i\zeta}\right\rangle_{(x,y,\tilde{z},\tau)} \quad , \tag{12}$$

where $j = 8\pi^2 Ne^2K^2L^2\rho/\gamma^3mc^2$ and $a = |a|\exp(i\phi)$. If the electron pulse is long, the spatial dependence can be dropped and a simplified wave equation,

$$\overset{o}{a} = -j\left\langle e^{-i\zeta}\right\rangle \quad , \tag{13}$$

is obtained. The solution for the linear undulator follows the same procedure except that K is replaced by $K\left(J_0(\xi) - J_1(\xi)\right)$, where $\xi = K^2/2(1+K^2)$ [3].

D. (LOW GAIN) FEL OSCILLATOR DESIGN

The pendulum equation and wave equations derived previously form a self-consistent Maxwell-Lorentz FEL theory. The dimensionless current density, j, couples the electron beam to the optical wave and is proportional to the change in the optical field. This theory is valid for strong or weak fields, $a \geq \pi$ or $a \leq \pi$ respectively, and high or low current, $j \geq \pi$ or $j \leq \pi$ respectively. [3]

An FEL oscillator generally operates in the weak field, low current regime. This design makes use of multiple passes to achieve gain and saturation. One method of achieving multiple passes is by reflecting light inside a resonator cavity as Figure 1 shows. In this case, one of the mirrors would have to allow some light out. Typically this is done with a hole in the center of the mirror or a partially transparent mirror.

Low current density, j, means there is a small change in the field a over a single pass. In the limit of low current density the field a can be assumed to be roughly constant and the integral of the pendulum equation, (7), becomes simple and yields,

$$\nu^2 = 2|a|\sin(\zeta + \phi) + 2H_0 \quad . \tag{14}$$

H_0 is a constant of motion resulting from the conservation of energy, and is called the Hamiltonian. The electron phase velocity is defined as $\nu = \overset{o}{\zeta} = L\left[\left(k + k_0\right)\beta_z - k\right]$. A weak field generally means that there is little change in the electron phase velocity over the undulator. Therefore, in weak fields with low current the solution to the pendulum equation, (7), can be given by [3]

$$\zeta(\tau) = \zeta_0 + \nu_0\tau - \frac{a_0}{\nu_0^2}\left[\cos(\zeta_0 + \nu_0\tau) - \cos(\zeta_0) + \nu_0\tau\sin(\zeta_0)\right] + \ldots \tag{15a}$$

and

$$\nu(\tau) = \nu_0 + \frac{a_0}{\nu_0}\left[\sin(\zeta_0 + \nu_0\tau)\right] + \frac{a_0^2}{\nu_0^3}\left[-\frac{1}{4}\left(\cos(2\zeta_0 + 2\nu_0\tau) - \cos(2\zeta_0)\right) - 1 - \nu_0\tau\sin(\zeta_0)\cos(\zeta_0 + \nu_0\tau)\right] + \ldots \quad (15b)$$

where ζ_0 is the initial electron phase, a_0 is the initial dimensionless optical amplitude and ν_0 is the initial phase velocity.

Near resonance small changes in the phase velocity are given by $\Delta\nu = 4\pi N\Delta\gamma / \gamma$ and changes in phase are given by $\Delta\zeta \approx k\Delta z$. These equations relate ν and ζ of (15) to the electron energy and the microscopic position of the electron in the beam. Phase space evolution is an ideal way to track electron dynamics and bunching. The electrons enter the phase space with (ν_0, ζ_0) and then evolve according to (14). The specific phase space path of an electron is given b e constant H_0 [3]. The initial phase velocity is determined from the resonance condition discussed earlier, where $\nu_0 = 0$ at resonance.

Phase space is most simply understood by tracking the familiar motion of an undriven pendulum. The points $(-\pi/2, 0)$ and $(3\pi/2, 0)$ are unstable fixed extrema and correspond to a pendulum at the top of its arc. The point $(\pi/2, 0)$ is a stable fixed extrema and corresponds to a pendulum at the bottom of its arc. In other words if a pendulum was released with no drag and allowed to swing back and forth it would trace out a closed orbit. Suppose this pendulum could come infinitely close to vertical in its swing path back and forth. This would trace out a path called the separatrix. The separatrix separates open orbits from closed orbits and is indicated by the solid line in Figure 3. However, if

the pendulum was given enough initial force to propel it over the top in a circular orbit it would correspond to an open orbit, one outside the separatrix. Setting $H_0 = 0$ in (14) gives the equation of the separatrix. It is evident that the height of the separatrix is $4\sqrt{|a|}$.

Phase space plots are particularly useful in determining FEL operation by following the evolution of the electrons. A single 2π section of the phase space is adequate because it is identical to others nearby when the coherence length of the optical wave is long [3]. When looking at a phase plot, it is important to realize that electrons near $\zeta = \pi$ transfer energy to the optical wave and those near $\zeta = 0$ take energy away from the optical wave. The phase velocity for maximum gain is $v_0 = 2.6$ [3].

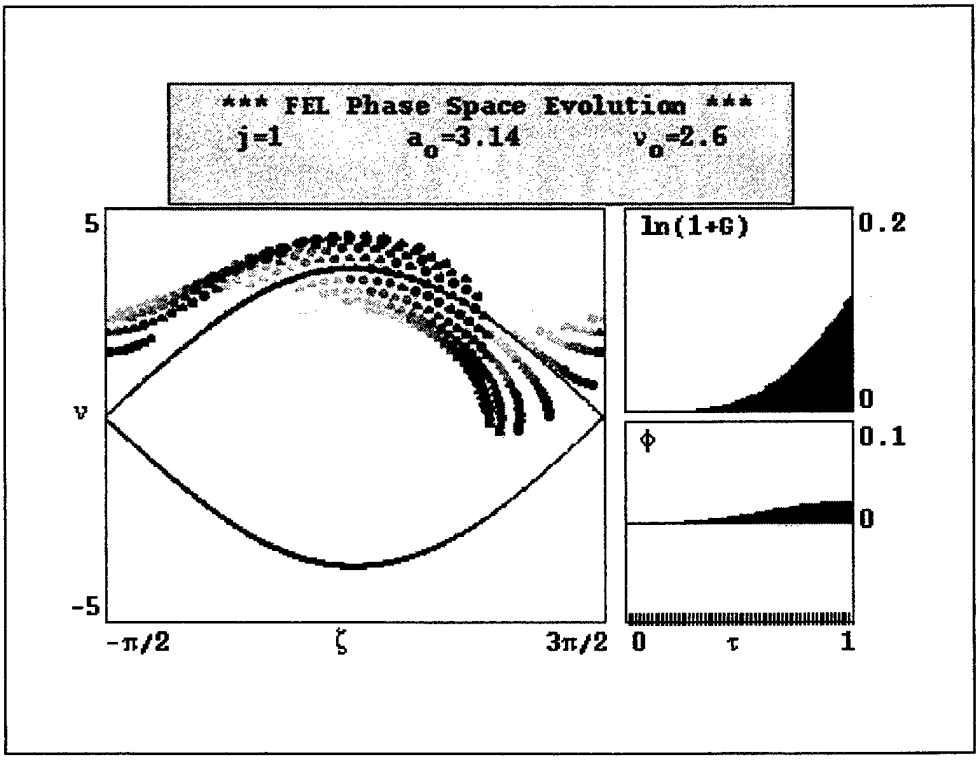

Figure 3. Electron phase space plot with low current and weak fields.

Figure 3 is a phase space plot of electrons through an undulator with a weak field and low current density created by solving the pendulum equation, (7), and the wave equation, (13). The electrons are injected into the undulator with uniformly spaced phases and initial phase velocity $\nu_0 = 2.6$. Normally there would be some spread in the phase velocities, but for this example it was assumed to be negligible. The initial position of the electrons is light grey and the positions get darker as the end of the undulator is reached. Electrons that initiate outside the separatrix stay in open orbits and those initially inside stay in closed orbits. The electrons bunch near $\zeta = \pi$, and therefore have significant gain, G, which is plotted to the right with the optical phase, ϕ with respect to τ. At the beginning of the undulator, there is little gain or phase change, but as bunching develops toward the end the gain and phase increase.

For low current and weak fields, energy conservation can be used to calculate the gain by equating the radiation energy of a volume of light with the energy lost from a volume of electrons. Electrons uniformly distributed in phase that are monoenergetic have an average energy loss of $\gamma mc^2\left(\langle\nu\rangle - \nu_0\right) / 4\pi N$. The first-order terms from (15) average to zero, but the second-order terms allow the gain to be written as

$$G(\tau) = jF\left(\frac{2 - 2\cos(\nu_0\tau) - \nu_0\tau\sin(\nu_0\tau)}{\nu_0^3}\right) \quad , \tag{16}$$

where $F = \left(r_b / w_0\right)^2$ is the "filling factor". Here r_b is the electron beam radius and w_0 is the optical mode radius. The gain is defined as the fractional increase in power contained in the optical field. In general, the interaction within the FEL changes both the amplitude

and phase of the optical field. Using the expansions given by (15) the wave equation, (13), can be solved and in lowest order of a_0 and j given by

$$|a(\tau)| = a_0\left(1 + j\left(\frac{2 - 2\cos(\nu_0\tau) - \nu_0\tau\sin(\nu_0\tau)}{2\nu_0^3}\right)\right) + \ldots \tag{17a}$$

and

$$\phi(\tau) = j\left(\frac{2\sin(\nu_0\tau) - \nu_0\tau(1 + \cos(\nu_0\tau))}{2\nu_0^3}\right) + \ldots \quad . \tag{17b}$$

In this weak-field low current case, the gain is dependent only on the current density and the initial phase velocity [3].

E. (HIGH GAIN) FEL AMPLIFIER DESIGN

The amplifier design usually makes use of high gain in a single pass. The components are similar to the oscillator design except that there is no resonator or feedback loop. In order to achieve high gain, amplifiers generally operate in a high current density regime with long undulators.

As the current density is increased, $j >> \pi$, the optical phase change and optical amplitude change are no longer small. The solution to the pendulum equation, (7), given by (15) is not valid in this regime. However, the pendulum and wave equations (7) and (13) are valid in the high gain regime so they can be solved numerically to explore the phase space evolution of the electrons. Figure 4 shows the evolution resulting from a current density of $j = 100$ and uniformly spaced electrons with an initial phase velocity of $\nu_0 = 1.6$, which corresponds to maximum gain in this case [3]. Like the low current

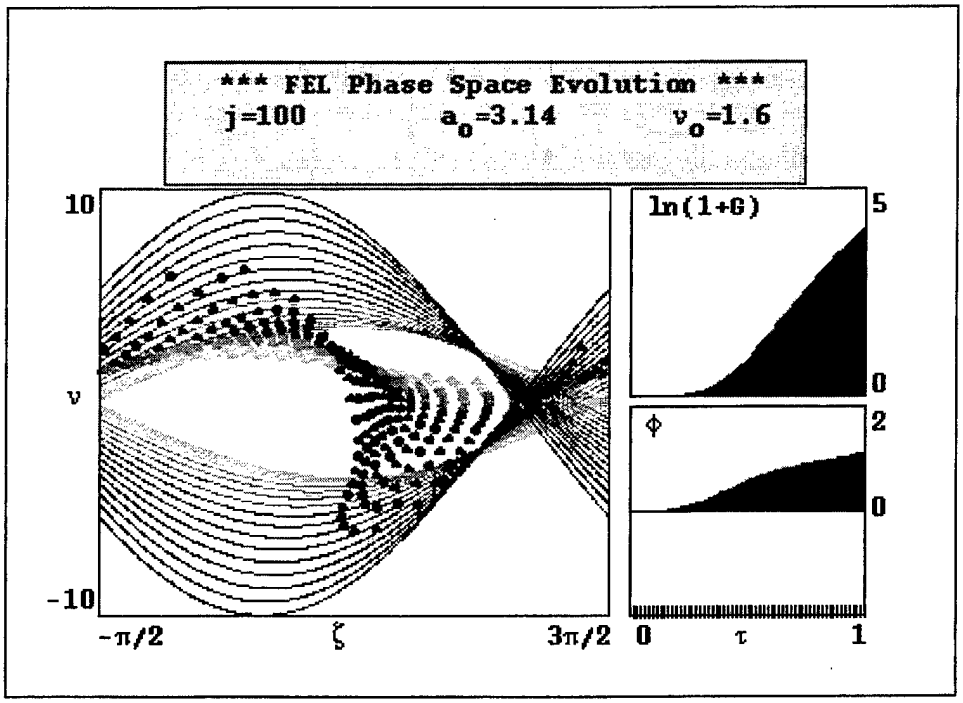

Figure 4. Electron phase space plot with high current and weak fields.

density plot in Figure 3, there is little bunching near the beginning of the undulator, $\tau = 0$, and therefore little gain or phase change. In this example, the beam is near resonance so the optical phase begins to grow without the corresponding increase in optical amplitude. This causes the separatrix to shift toward $\zeta = \pi$ and high gain begins. The high gain in this example causes the height of the separatrix to increase dramatically. Figure 4 shows the evolution of the separatrix from light grey to black as the electrons move along the undulator from $\tau = 0$ to $\tau = 1$.

In this high current, weak field regime, the wave and pendulum equations can also be solved analytically using perturbation theory. The expanded wave and pendulum

equations can be combined and integrated over all initial phases, $\int d\zeta_0$, to obtain the following equation governing the evolution of the optical field [3]

$$\overset{o}{a}(\tau) = \frac{ij}{2}\int_0^\tau d\tau'\tau' F(\tau') e^{-i\nu_o\tau'} a(\tau-\tau') \quad , \tag{18}$$

where $F(\tau') = \int dq f(q) e^{-iq\tau'}$ is the characteristic function of the distribution of the initial electron phase velocities, *f(q)*. In (18), reference to electron phases has been removed, but there is an average over the distribution of initial electron phase velocities. Equation (18) is valid in weak fields with high or low current density. The form of the solution can be found by taking successive derivatives. After finding the roots to the characteristic equation and applying initial conditions the solution,

$$a(\tau) = \frac{a_0}{3}\left[e^{(j/2)^{1/3}(i+\sqrt{3})\tau/2} + e^{(j/2)^{1/3}(i-\sqrt{3})\tau/2} + e^{-i(j/2)^{1/3}\tau} \right] \quad , \tag{19}$$

is found. This shows that for small τ, there is little change in the optical field amplitude. This remains true during the bunching time, $\tau < \tau_B \approx (2/j)^{1/3}$. As soon as the electrons bunch there is exponential growth and high gain. In the high current limit, the fastest growing term from (19) dominates, and the solution to the wave equation, (13) is given by

$$\begin{aligned} |a(\tau)| &\approx \frac{a_0}{3} e^{(j/2)^{1/3}\sqrt{3}\tau/2} \\ \phi(\tau) &\approx (j/2)^{1/3}\tau/2 \end{aligned} \quad . \tag{20}$$

For high current, the optical gain is given by

$$G(\tau) = \frac{1}{9} e^{(j/2)^{1/3}\sqrt{3}\tau} \quad . \tag{21}$$

In order to obtain the solutions given in (18) and (19), perfect beam quality and initial phase velocity, $\nu_0 = 0$, were assumed.

1. The Tapered Undulator

As electrons give up energy to the optical wave and slow down they begin to drop out of the gain spectrum. This is a problem in the amplifier design since it is important to get the maximum energy out of the electrons in a single pass. It would be ideal if the electrons could be accelerated to stay in the gain spectrum. Resonance would then be maintained and the interaction between the electrons and the optical wave would be allowed to continue.

There are two basic methods for replacing or compensating for the electron's lost energy. They are evident if one looks at the resonance condition, (5). The electron losing energy means that γ is decreasing. This means that either the "undulator parameter ", K, or the undulator wavelength, λ_0, must decrease to maintain resonance. Decreasing the undulator wavelength along the z axis means decreasing the spacing between the magnets as the electron progresses fro the beginning to the end of the undulator. This results in an artificial acceleration of $\delta \approx -2\pi N \Delta\lambda_0 / \lambda_0$, where N is the number of periods and λ_0 is the undulator wavelength. Another method is to decrease K, which is directly proportional to the undulator field strength, along the z axis giving an artificial acceleration of $\delta \approx -4\pi N K^2 \Delta B / B\left(1+K^2\right)$, where B is the magnetic field amplitude. Figure 5 demonstrates these concepts. The arrows represent magnetic field inside the undulator, where a shorter arrow means a smaller field. The untapered undulator is represented by A. B and C represent tapering the magnetic field and undulator wavelength respectively. With tapering included (7) and (13), the pendulum and wave

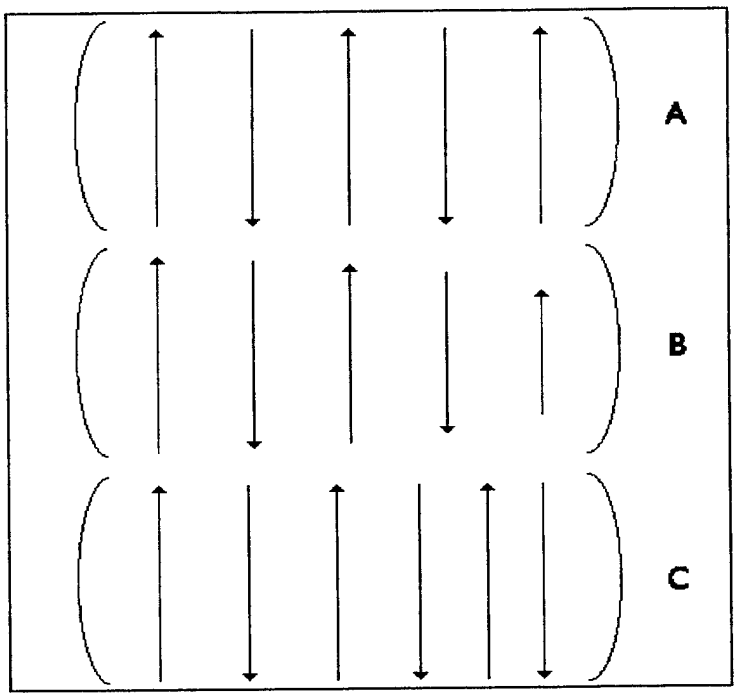

Figure 5. Methods of tapering.

equations become

$$\overset{oo}{\zeta} = \overset{o}{\nu} = \delta + |a|\cos(\zeta + \phi) \text{ and } \overset{o}{a} = -j\langle e^{-i\zeta} \rangle \quad , \tag{22}$$

where $\zeta = \int_0^{\tau} k_u(\tau')d\tau' + kz - \omega t$ [3]. These equations are valid for weak and strong optical fields with either high or low gain, but not when efficiency is large, $\eta \approx 10\%$ or more.

Tapering can be advantageous when the artificial acceleration δ exceeds the deceleration obtained without taper in strong optical fields. The desirable criteria for tapering is given by

$$|a| > \delta \geq 4|a|^{1/2} \geq 2\pi \quad , \tag{23}$$

where the left side of this inequality is the condition for trapping electrons in tapered phase space. The middle describes the condition that the artificial acceleration exceeds the

deceleration. The right side is the condition that the taper operate in the strong field regime.

Electrons in the tapered undulator evolve a bit differently in phase space than in the untapered undulator. Electrons with an initial phase of $\zeta_0 = 0$ are accelerated by both the optical field, $|a|$, and the artificial acceleration, δ, and will eventually contribute little to the interaction between the optical wave and the electron beam. Electrons with an initial phase of $\zeta_0 = \pi$ see the forces of δ and $|a|$ roughly cancel out leaving them trapped in closed orbits. From this perspective, it is easy to see that tapering works because electrons which give energy to the optical wave are trapped and those which take energy from the optical wave are accelerated away.

Tapering the undulator leads to much higher efficiency and gain in strong optical fields, but has lower gain in weak optical fields. When the taper rate, or phase acceleration, δ is too large for the FEL field strength, electrons will not remain trapped and efficiency is reduced. Figure 6 is a phase space plot of 1000 electrons in an initial strong field of $a_0 = 40$ that is amplified by a current $j = 1$. The initial phase velocity is zero and the taper rate is $\delta = 10\pi$ which meets the criteria of the (23). From this figure it is evident that the untrapped electrons are spread fairly evenly in phase, and the trapped electrons are concentrated inside the separatrix in the area for gain. Electrons can be seen to leak out of the separatrix on the right side due to the growth in optical amplitude and a shifting phase, ϕ. The oscillations in the gain and phase plots on the right are due to the revolution of the electrons inside the separatrix. Examination of Figure 6 reveals that about 50% of the electrons are trapped. As it turns out the efficiency of this tapered

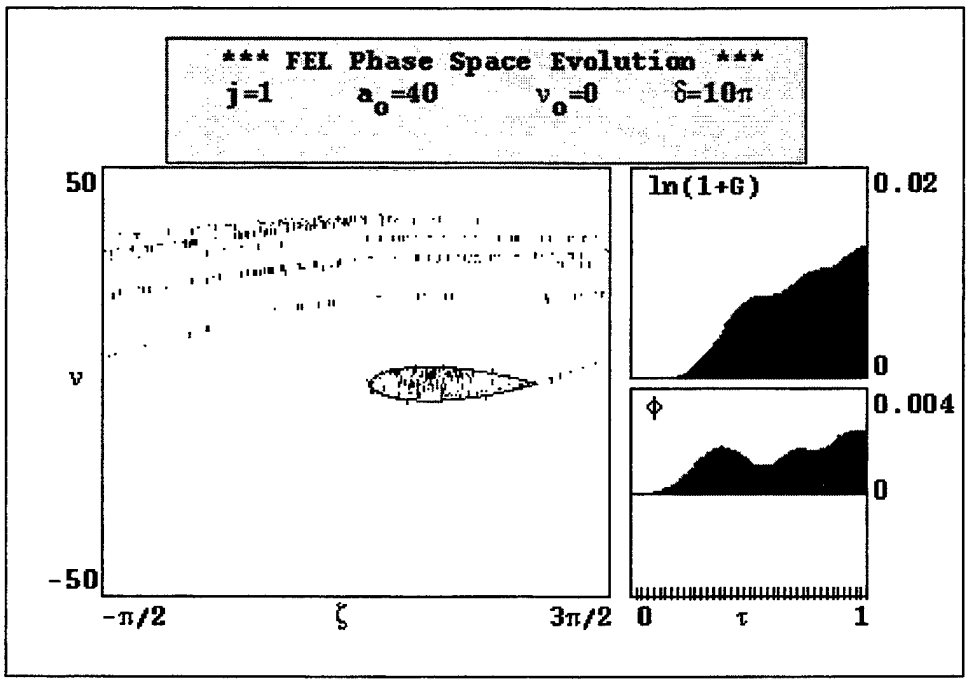

Figure 6. Tapered undulator phase space plot with low current.

undulator is about 3 times the natural efficiency without taper [3]. Increasing the current traps more electrons and the gain increases even more significantly.

2. The Regenerative Amplifier FEL (RAFEL)

LANL has demonstrated a combination of the oscillator and amplifier designs called the RAFEL shown in Figure 7. The device is designed to operate in the high current, high gain regime, but uses a small amount of feedback. The photoinjector injects the electrons into the linear accelerator and then they pass through a hole in the first mirror. The electrons in the undulator give up energy to the optical wave. The beam is then guided through a hole in the second mirror at the end of the undulator and is directed into a beam dump. Most of the optical wave passes through the same hole in the mirror,

but a small fraction is recirculated through a feedback loop to the beginning of the undulator to be amplified by the subsequent incoming electrons. While feedback is a characteristic of oscillator designs, the concept behind the RAFEL's feedback is fundamentally different. The purpose is only to seed the FEL with a small amount of power so that the process does not start from noise. The high single-pass gain overcomes the small amount of feedback. This allows the RAFEL to reach saturation in only a few passes. Details of the RAFEL design will be discussed in the next chapter.

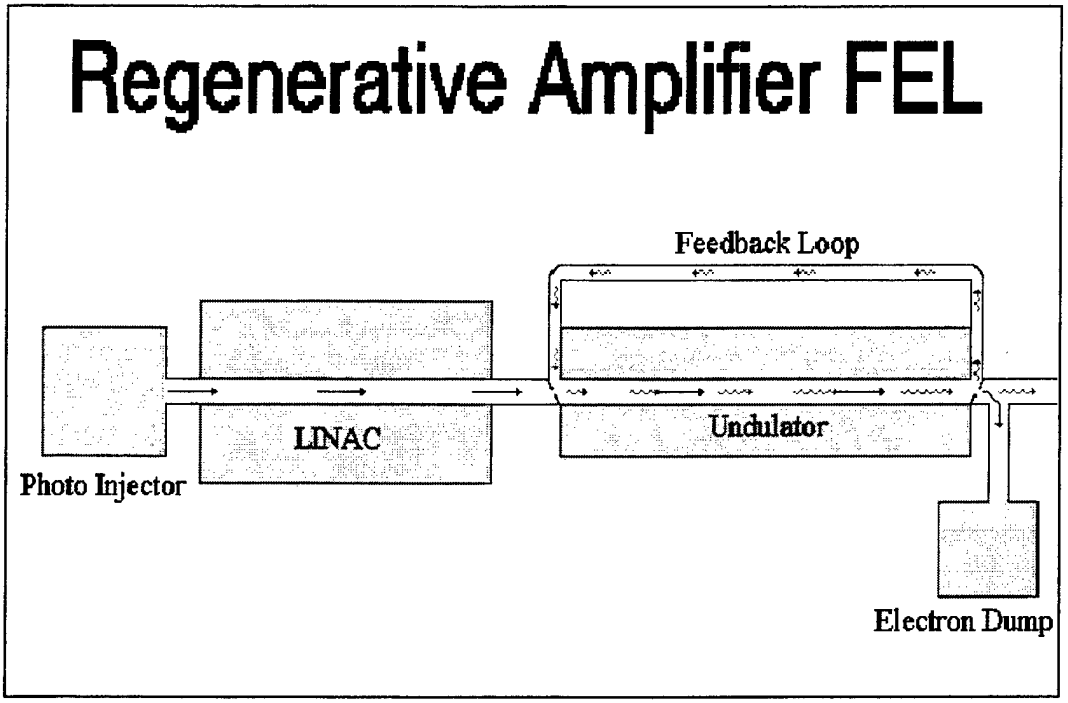

Figure 7. Diagram of the Regenerative Amplifier FEL.

F. 3D DIFFRACTION

Any freely-propagating, coherent optical wave will spread due to natural diffraction as it passes through the undulator. The Rayleigh range, $\pi w_0^2 / \lambda$, is defined as

the distance over which light of wavelength, λ, initially doubles in transverse area. The initial area of the optical wave is given by πw_0^2. It is important to ensure that the Rayleigh range is comparable to the length of the undulator, L, or FEL coupling could be reduced by diffraction of the wave away from the electron beam. This occurs if the optical mode becomes significantly larger than the electron beam. If the current density is high enough, this restriction on the Rayleigh range can be modified because the radiation wavefront is distorted, or guided, by the electron beam.

FEL optical guiding can occur when the high-current-density electron beam continually focuses the optical light wave back into the electron beam. The optical phase evolution along the undulator is $d\phi_j = \left(jr_e^2 / 2w_0^2\right)^{1/3} dz / 2L$. This includes the "filling factor" discussed previously. Natural diffraction produces a phase shift $d\phi_D = -dz\lambda / \pi w_0^2$ which is of the opposite sign. In order for the FEL to have optical guiding $d\phi_j \geq d\phi_D$. From this inequality, it is evident that either a high j or a large electron beam are necessary for effective guiding of the optical mode. [6]

The FEL theory developed earlier can be extended to include transverse modes. The complex optical field envelope is still taken to be slowly varying along z. The derivation is essentially the same as before. The transverse coordinates can be normalized to the characteristic mode size, $x\sqrt{\pi / L\lambda} \rightarrow x$ and $y\sqrt{\pi / L\lambda} \rightarrow y$, where L is the length of the undulator and λ is the optical wavelength. The longitudinal coordinate can be normalized to the slippage distance, $(z - ct / N\lambda) \rightarrow z$, where c is the speed of light and N

is the number of periods in the undulator. Then using dimensionless time, $\tau = ct / L$, the parabolic wave equation can be written as

$$\left[-\frac{i}{4}\nabla_{\perp}^{2} + \frac{\partial}{\partial\tau}\right] a(x, y, z, \tau) = -\left\langle je^{-i\zeta}\right\rangle_{(x,y,z,\tau)} \quad , \tag{24}$$

where $\nabla_{\perp}^{2} = \partial_x^2 + \partial_y^2$ [3]. This equation governs the dynamics of the optical wave in the z direction as before, and the $\nabla_{\perp}^{2}$ operator describes diffraction in the transverse (x, y) directions. The solution to (24) is given by

$$a(x, y, z, \tau + \Delta\tau) = \exp\left(\frac{i\Delta\tau}{4}\nabla_{\perp}^{2}\right) a(x, y, z, \tau) - \Delta\tau\left\langle je^{i\zeta}\right\rangle_{x,y,z-\tau,\tau} + \ldots \tag{25}$$

to order $j\Delta\tau^2$ [3]. The evolution of the electron current is governed by the Lorentz force equation for each electron in the beam. The pendulum equation can be generalized to the form

$$\overset{o}{v}(x, y, z-\tau, \tau) = \overset{oo}{\zeta}(x, y, z-\tau, \tau) = \left|a(x, y, z, \tau)\right| \cos\left[\zeta(x, y, z-\tau, \tau) + \phi(x, y, z, \tau)\right] \tag{26}$$

to complete the theory in 4 dimensions [3].

G. TRAPPED PARTICLE INSTABILITY

When saturation is reached in a strong field, the height of the separatrix is large and the electrons tend to travel in closed phase space paths causing increased efficiency. While in these closed paths, some electrons become trapped in deep potential wells. This results in decreased bunching and decreased gain. This effect is termed the "trapped-particle instability." It occurs when an FEL evolves to power levels beyond saturation.

The oscillations of the trapped electrons starts the instability and for electrons near phase ζ_0 the motion is described by

$$\zeta(\tau) = \zeta_0 + \frac{\nu_0}{\nu_s}\sin(\nu_s\tau) \quad , \tag{27}$$

for the initial position (ζ_0, ν_0) [3]. The trapped-particle oscillation frequency, or "synchrotron" frequency, is given by $\nu_s = \left(|a|^2 - \delta^2\right)^{1/4}$. The taper parameter, δ, is zero when the undulator is not tapered. Sidebands appear at $\nu_0 \pm \nu_s$ away from the fundamental wavelength by $\Delta\lambda / \lambda = \nu_s / 2\pi N$. The shift is simply the ratio of the number of synchrotron oscillations to the number of periods in the undulator.

H. SHORT PULSE EFFECTS

When the electron beam is made up of short pulses, comparable in length to the slippage distance $N\lambda$, the interaction between the optical wave and the electron beam will be dominated by short pulse effects. A series of short electron pulses generates a series of short optical pulses. In the oscillator design these optical pulses bounce between the resonator mirrors separated by a distance S. The reflected optical pulse arrives at the beginning of the undulator in time intervals, $2S / c$, and the entering electron pulses must be synchronized to arrive at the same times. Desynchronism, d, is the displacement between the electron and optical pulses at the beginning of the undulator. Desynchronism, d, is normalized to the slippage distance so that when $d = 0$ there is exact synchronism.

The light pulse drifts away from the electron pulse over many passes when there is exact synchronism. This effect is due to the light pulse being distorted on each pass

because gain is preferentially added to the trailing edge of the pulse. This causes the effective speed of the pulse to slow and fall away from the bunched electrons. The end result over many passes is no gain. The desynchronization can be controlled by adjusting the path length or reducing the distance between mirrors.

At small desynchronism, the optical power can be large enough to cause trapped-particle instability, creating a broad optical spectrum and a broad electron spectrum. The trapped-particle instability is identified by sharp spikes in the optical pulse. Since a small change in d causes a large change in steady-state power, the FEL is generally unstable at small values of desynchronism. The FEL becomes more stable for larger values of d in the operating range. The reduced coupling at larger d causes lower steady-state power, and therefore trapped-particle instability generally does not occur. The power spectrum is narrow because the optical pulse is smooth and longer than the electron pulse. [3]

Another effect of short pulses is "limit cycle behavior" in the optical pulse. This behavior is represented by the power and optical pulse oscillating periodically over many passes. Limit cycle behavior occurs at values of d where a stable laser pulse configuration does not occur. The structure initiates on the trailing edge of the optical pulse and the desynchronism mechanism forces it through the pulse envelope. [3]

III. RAFEL DESIGN

A. INTRODUCTION

As mentioned previously, the LANL RAFEL is a combination of the oscillator and amplifier designs. The term regenerative amplifier was coined for this design because it is similar to conventional laser regenerative amplifiers. The optical feedback is only on the order of 10^{-2} to 10^{-5} . As a consequence of the electron beam pulse structure, shown in Figure 8, the optical feedback path must be synchronized with the incoming electron beam to ensure there is overlap. The advantage of this type of FEL design is that the mirrors never get exposed to high peak or average power. [6]

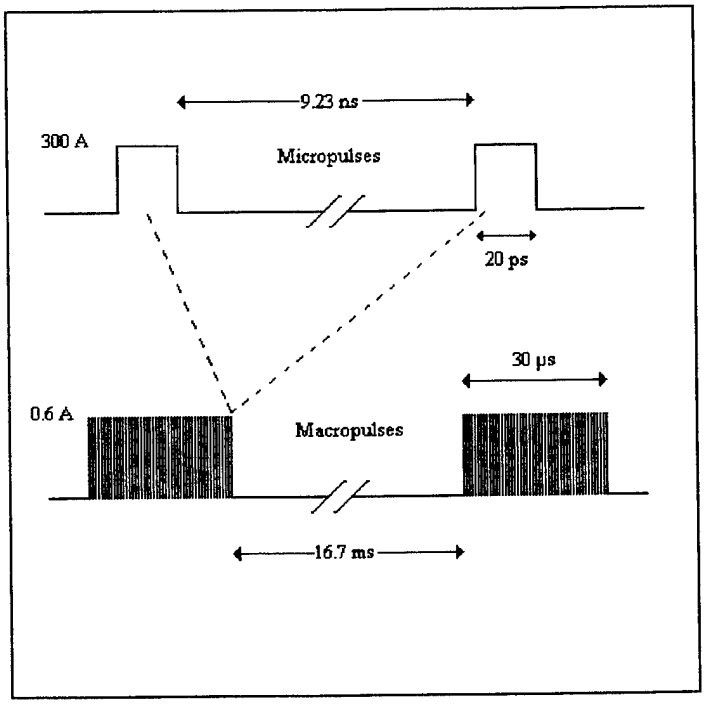

Figure 8. Pulse structure of LANL RAFEL [6].

B. LANL RAFEL SYSTEM CHARACTERISTICS

1. The Electron Beam

The rf power source provides an output greater than 20 MW peak for 30 microseconds. The average power of the 1300 MHz klystron transmitter is 50 kW in bursts [6]. This powers a photoinjector/linac which creates a beam of electrons with an energy of 17 MeV, 300 A micropulses at approximately 100 MHz. The current macropulse repetition rate is only 1 Hz, but 60 Hz will be available when diode-array-pumped amplifiers are installed. Details of the pulse structure are shown in Figure 8. The duty factors for the micropulse and macropulse are on the order of 0.2% [6]. This combined with the 300 A peak current and 17 MeV electron beam leads to the predicted kW output power. Multiplying the beam energy by the true average current gives; $17 \times 10^6 V \times 300 A \times 0.002^2 \approx 20 kW$. This value multiplied by the efficiency gives the output power. If an efficiency of 5% can be achieved, this would give an output of 1 kW. The relatively high current density could cause guiding of the optical mode which would be favorable to FEL coupling. However, the small electron beam has a small radius of only 0.18 mm could reduce this effect.

2. The Undulator

The undulator is $L = 2$ meters long with a $\lambda_0 = 2$ cm period. Each period contains four permanent magnets in a modified Halbach configuration [6]. The first meter of the undulator is untapered while the last meter has about a 30 % taper in the undulator field. The undulator gap in the first meter is 0.59 cm. In order to accommodate the growing

optical mode the taper is accomplished by increasing the gap between the magnets to effectively reduce the magnetic field that the electrons experience. This is accomplished by increasing the undulator gap to 0.95 cm by the end of the tapered section of the undulator. The undulator period remains constant throughout the undulator. Two plane focusing is accomplished with a rectangular groove cut on the pole face of the magnets and is equal strength in both directions.

3. Feedback Loop

The feedback loop consists of mirrors as shown in Figure 9. The annular mirrors are relatively flat with the upstream mirror having a 0.25 cm hole in the center and the downstream mirror having a 0.70 cm hole in the center. These holes allow the electron beam to pass through unimpeded. The downstream mirror has a larger hole to allow the portion of the optical mode centered near the electron beam to pass through. The outer portion of the mode is reflected back through spherical and cylindrical mirrors to seed the

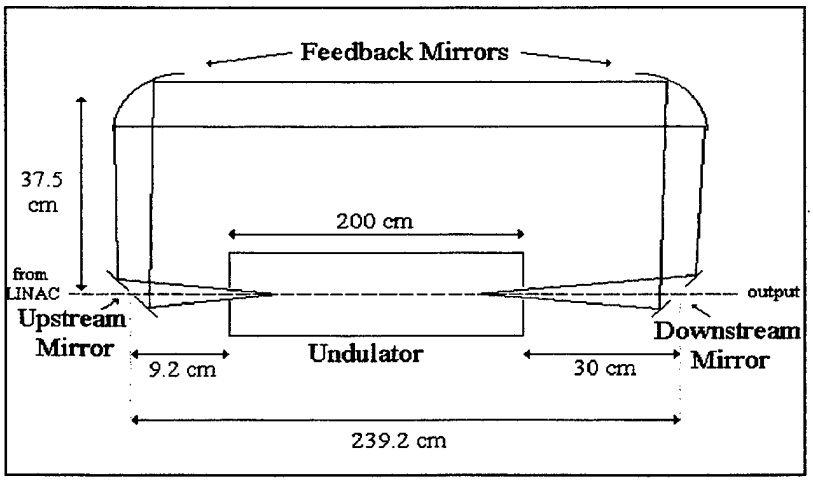

Figure 9. Feedback loop for LANL RAFEL [6].

undulator. Therefore, in order for the design to function as anticipated, a small amount of the optical field in a donut shape feeds back enough light to continually seed the undulator. The large-signal optical field concentrated around the electron beam provides outcoupling. The detuning length for the RAFEL design is longer than conventional FEL designs and must be within 6 mm of the 20 ps electron pulse length to observe lasing.

C. SYSTEM PARAMETERS

Table 1 is a summary of some significant electron beam and undulator parameters used for the simulations in the following chapter. The experiment was set up for a peak current of 300 A. A peak current of 370 A is possible in the future so some simulations were conducted at that current for comparison. The undulator parameter listed in the table is given by $K = eB_{rms}\lambda_o / 2\pi mc^2$, where λ_o is the undulator wavelength or period. From the resonance condition presented earlier, $\lambda = \lambda_o\left(1+K^2\right)/2\gamma^2$, the expected optical wavelength of the RAFEL is about 16 μm.

Electron Beam Parameters		Undulator Parameters	
Electron kinetic energy	17 MeV	Length	2 m
Micropulse length	18 ps	Period (wavelength)	2 cm
Beam radius	0.18 mm	Magnetic field amplitude	0.7 T
Emittance	5 mm-mrad	Undulator parameter	0.92
Peak current	300 - 370 A	Magnitude of taper	30.25%
Fractional energy spread	0.1%	Taper starts at	1 m

Table 1. LANL RAFEL parameters.

IV. SIMULATIONS

A. INTRODUCTION

This chapter discusses simulations of the RAFEL. The parameters of the LANL experiment are explored in order to develop a better understanding of the physics behind the RAFEL design. The goal in exploring the LANL parameters is to examine the feasibility of reaching a kW and to optimize a few of the parameters. In support of this, the taper rate and feedback amount were optimized using a simulation including diffraction in three dimensions (x,y,t), but not taking into account longitudinal pulse effects and slippage. The same simulation was used to explore the maximum efficiency versus the initial phase velocity, ν_o. In order to enhance understanding of the RAFEL concept, simulations including pulse effects and multiple passes were performed without diffraction. Further simulations were performed without diffraction and using a perfect beam to idealize the full potential of the RAFEL concept.

B. TAPER OPTIMIZATION

Three dimensional (3D) simulations were used to explore the effects of diffraction in the undulator with varying taper rate δ. The LANL RAFEL is constructed with the taper starting halfway through the undulator. Figure 10 shows the output of a 3D diffraction simulation with a peak current of 300 A and feedback of 10^{-4}. The taper rate in this case is $\delta = 128\pi$ corresponding to the design taper listed in Table 1. Recall that the undulator length indicated by τ goes from zero to one.

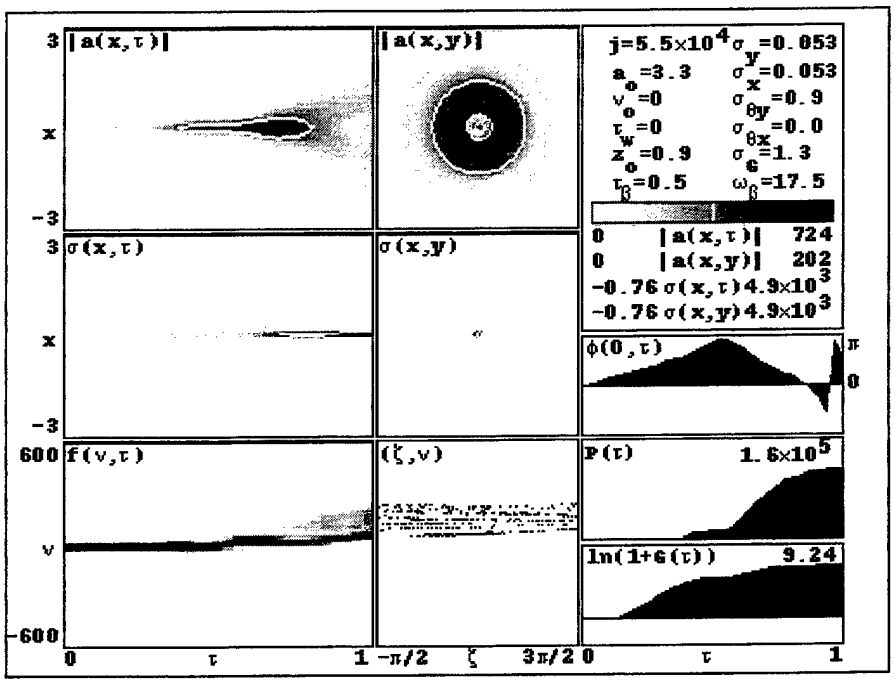

Figure 10. 3D RAFEL simulation with $\delta = 128\pi$.

The evolution of the optical mode, $|a(x,\tau)|$, shown in the upper-left window of Figure 10, is dominated by diffraction after the taper is turned on at $\tau = 0.5$. The intense electron beam provides guiding over the first meter of the undulator, $\tau < 0.5$, but diffraction overcomes this focusing over the last meter of the undulator where $\overset{\circ}{\phi}(\tau) < 0$. The window in the top-center shows a cross-sectional view of the optical mode, $|a(x,y)|$, at the end of the undulator. The top-right window lists the dimensionless parameters for this simulation; $a_0 = 3.3$ is the initial dimensionless optical amplitude, $j = 5.5 \times 10^4$ is the dimensionless beam current density, $\sigma_x = \sigma_y = 0.053$ corresponds to the dimensionless radial size of the electron beam, and $\sigma_{\theta y} = 0.9$ and $\sigma_G = 1.3$ characterize beam quality. The random Gaussian spread of the electrons is σ_G and the spread in angle is $\sigma_{\theta y}$. The graph at the right-middle shows the development of the optical phase along the undulator

length $\phi(\tau)$. When the taper turns on at $\tau = 0.5$, the optical phase change along the undulator length becomes negative $\dot{\phi}(\tau) < 0$ and encourages the optical wavefront to be excluded from the electron beam, thus decreasing the interaction strength. The lower-right is the plot of the dimensionless optical power growth along the undulator $P(\tau)$ and the plot of the natural logarithm of the single-pass gain along the undulator $ln(1+G(\tau))$. The middle-left window shows the bunching current development in the electron beam along the undulator, with the end view in the center. This is indicated by the appearance and darkening of a line, indicating bunching current, in the center of the plot. At the bottom-left is the beam's electron phase velocity evolution along the undulator, and the bottom-center is the beam's electron phase space plot at the end of the undulator.

In order to optimize gain and efficiency for an FEL, about 50% of the electrons should be trapped [4]. In Figure 10, much less than half the electrons are trapped near resonance $\nu = 0$ as can seen in the bottom-center photo where there is no significant bunching, indicating the taper rate is too large causing electron detrapping.

δ	η	$P(\tau)$	G_f
80π	7.1%	$2.4\text{x}10^5$	$1.67\text{x}10^3$
90π	7.7%	$2.5\text{x}10^5$	$1.77\text{x}10^3$
95π	7.9%	$2.5\text{x}10^5$	$1.80\text{x}10^3$
100π	8.1%	$2.6\text{x}10^5$	$1.83\text{x}10^3$
110π	8.3%	$2.6\text{x}10^5$	$1.87\text{x}10^3$
112π	**8.3%**	**$2.6\text{x}10^5$**	**$1.87\text{x}10^3$**
115π	8.3%	$2.6\text{x}10^5$	$1.86\text{x}10^3$
120π	8.0%	$2.5\text{x}10^5$	$1.79\text{x}10^3$
128π*	6.5%	$2.2\text{x}10^5$	$1.52\text{x}10^3$
135π*	5.5%	$1.9\text{x}10^5$	$1.33\text{x}10^3$

Table 2. 300 A taper optimization results.

Table 2 summarizes the taper optimization results for a peak current of 300 A and an initial dimensionless optical amplitude of $a_0 = 10$. It was determined that for these parameters the optimum taper rate is $\delta = 112\pi$. This increased the efficiency and single-pass gain. The asterisk in the taper rate column indicates that the simulation included a hole was present in the center of the optical mode at the end of the undulator.

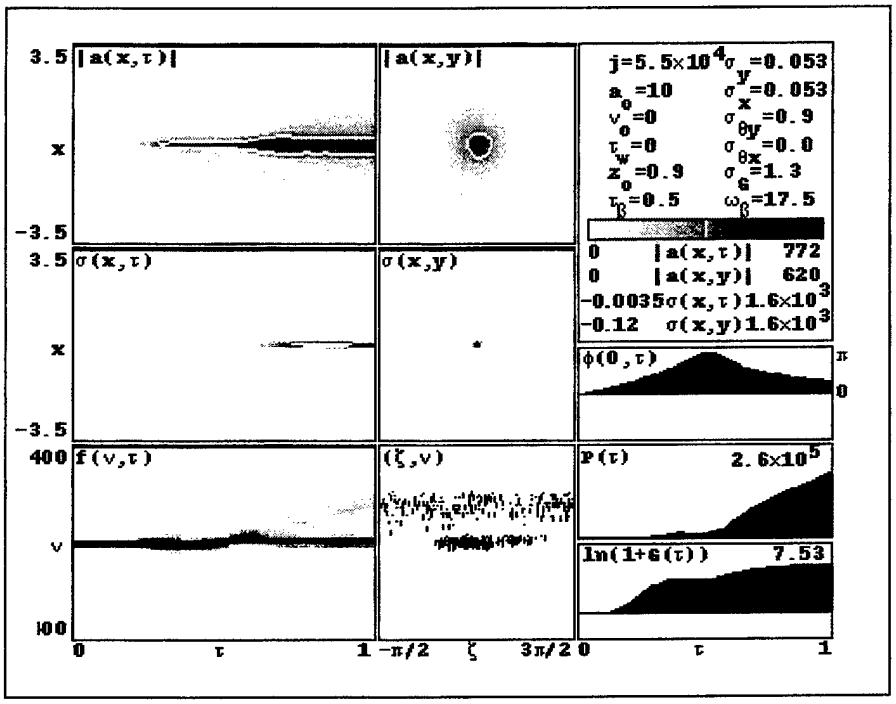

Figure 11. 300 A peak current simulation with $\delta = 112\pi$.

Figure 11 shows the results of the 3D diffraction simulation for the optimum taper rate determined from Table 2. Reducing the taper to $\delta = 112\pi$ allowed for continued guiding of the optical mode after the taper starts at $\tau = 0.5$. This is evident in the upper-left window which shows the majority of the optical power remains centered around the electron beam from $\tau = 0$ to $\tau = 1$. The upper-middle window also demonstrates improved

guiding, because no hole develops in the center of the optical mode. The bottom-middle window shows the bunched electrons trapped in the center of the phase-space plot. Note that around 50 % of the electrons remained trapped near resonance, $\nu = 0$, with the reduced taper of $\delta = 112\pi$. When the taper rate is too large, electrons cannot be captured by the optical field and are detrapped.

The same optimization was performed for a peak current of 370 A realizing an optimal taper rate of $\delta = 135\pi$, with results summarized in Table 3. This provided only a slight increase in efficiency and single-pass gain over the design taper of $\delta = 128\pi$. The higher beam current allows for increased optical guiding which enables larger taper values to be used effectively.

As can be seen in Figure 10, the optical mode has a hole in the final optical mode due to a loss of guiding of the optical mode along the undulator. Since the electron beam has a small radius of 0.18mm, a large current density is necessary for guiding. While guiding occurs initially, when the taper turns on halfway through, the undulator diffraction

δ	η	$P(\tau)$	G_f
90π	8.2%	$3.4\text{x}10^5$	$2.42\text{x}10^3$
100π	8.8%	$3.6\text{x}10^5$	$2.56\text{x}10^3$
110π	9.4%	$3.8\text{x}10^5$	$2.68\text{x}10^3$
120π	9.9%	$3.9\text{x}10^5$	$2.78\text{x}10^3$
130π	10.2%	$4.0\text{x}10^5$	$2.85\text{x}10^3$
135π	**10.3%**	**$4.1\text{x}10^5$**	**$2.86\text{x}10^3$**
140π	10.3%	$4.0\text{x}10^5$	$2.86\text{x}10^3$
145π	10.0%	$4.0\text{x}10^5$	$2.86\text{x}10^3$
150π	9.4%	$3.7\text{x}10^5$	$2.64\text{x}10^3$
155π*	8.2%	$3.3\text{x}10^5$	$2.37\text{x}10^3$

Table 3. 370 A taper optimization results.

effects begin to take over. The optical mode begins to grow and the slope in the optical phase is negative, indicating a loss of guiding. In order to prevent this, the taper rate must not be too large for a given peak current. In the case of the 300 A peak current, a decreased taper rate did not result in a hole in the center of the optical mode leading to a corresponding increase in efficiency and power output. The change in taper rate allowed for increased optical guiding in the second half of the undulator. Higher currents allow the use of a higher taper rate before diffraction effects overcome optical guiding. This is evident when comparing Table 2 and Table 3. The hole in the optical mode does not occur until $\delta = 155\pi$ for a peak current of 370 A, while at a lower current of 300 A the hole forms at a taper rate of only $\delta = 128\pi$.

C. EFFECTS OF FEEDBACK

Since this design is a cross between the oscillator and the amplifier, the amount of feedback could be essential in the understanding of the design. The RAFEL design uses only a small amount of feedback to seed the undulator. However, the amount of feedback for optimum efficiency has not been explored. In order to explore the effect of this aspect of the RAFEL, simulations varied the initial dimensionless optical field, a_0, from 1 to 130. The single-pass 3D simulation is used as a representation of steady-state in an oscillator with the initial optical field determined by the amount of feedback. The inverse of the single-pass gain G_f is the amount of the feedback for high gain, or small feedback, $f(G) = 1/\left(1+G_f\right)$. Therefore, the variation in feedback during the simulations ranged from about $f = 10^{-1}$ to $f = 10^{-5}$.

The amount of feedback throughout this range surprisingly had almost no effect on efficiency and final power, as shown in Tables 4 and 5. The efficiency for the 300 A case was $\eta = 7\% \pm 0.5\%$, while the efficiency for the 370 A case was again within 0.5% of the average value of $\eta = 10\%$. In both instances, saturation was reached because the output power was essentially the same due to the high gain at the beginning of the RAFEL undulator.

a_0	η	$P(\tau)$	G_f
1	7.2%	2.2×10^5	1.6×10^5
5	6.6%	2.2×10^5	6.1×10^3
10	6.5%	2.2×10^5	1.5×10^3
40	7.2%	2.4×10^5	106
70	6.9%	2.4×10^5	34
100	7.1%	2.5×10^5	17
130	7.5%	2.7×10^5	10

Table 4. Feedback optimization for a 300 A peak current.

a_0	η	$P(\tau)$	G_f
1	10.5%	4.0×10^5	2.8×10^5
5	9.9%	3.9×10^5	1.1×10^4
10	10.1%	4.0×10^5	2.8×10^3
40	10.7%	4.3×10^5	191
70	10.4%	4.3×10^5	61
100	10.2%	4.3×10^5	30
130	10.2%	4.4×10^5	17

Table 5. Feedback optimization for a 370 A peak current.

Figures 12 and 13 correspond to a peak current of 300 A and initial dimensionless optical amplitude of a_0=1 and a_0=130, respectively. These values cover the range of

feedbacks listed in Table 4, and represent feedback amounts on the order of $f = 10^{-5}$ for Figure 12 and $f = 10^{-2}$ for Figure 13. In Figure 12, diffraction effects dominate over the

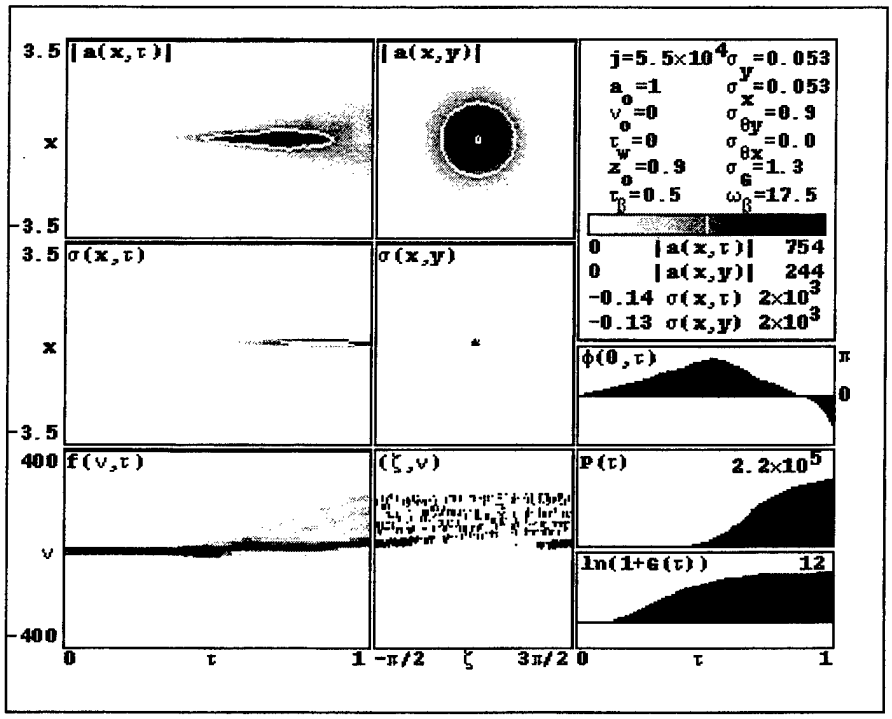

Figure 12. 3D simulation for 300 A and 10^{-5} feedback.

second half of the undulator resulting in a hole in the center of the optical mode. Also of note are the ineffecient trapping of electrons, and the significant change in phase over the last half of the undulator.

Figure 13 still shows the effects of diffraction of the optical mode along the undulator, but the majority of the mode is still centered around the electron beam at the end of the undulator with no hole developing in the optical mode. Notice that the phase change over the last half of the undulator is not as rapid, resulting in more efficient electron bunching.

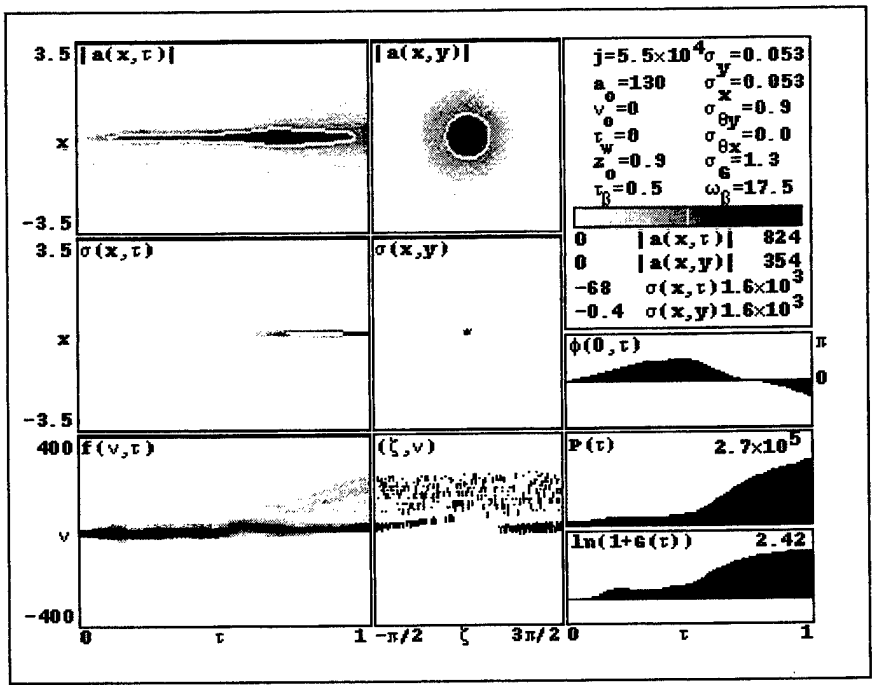

Figure 13. 3D simulation for 300 A and 10^{-2} feedback.

When looking at the dimensionless power and efficiency in Tables 4 and 5, it appears that feedback does not play a significant role in the design. However, on closer examination it is evident that the shape of the optical mode is significantly effected. As the amount of feedback increases the hole in the optical mode diminishes and even goes away. This is important because the RAFEL laser output is the amount of optical power which exits the undulator from a hole in the center of the downstream mirror. The optical power which does not exit is fed back to seed the undulator. This means that only the outer portion of the optical mode is used for feedback. Since the hole in the output mirror has a diameter of 14 mm, only a tiny fraction is used for feedback. In fact, if the optical mode did not diffract sufficiently there would be no feedback at all. If the hole in the mirror were smaller a larger amount of the optical mode could be fed back.

D. EFFECTS OF INITIAL PHASE VELOCITY

Because the RAFEL is actually an oscillator, the feedback used will allow the initial phase velocity to seek a maximum in gain. Since the initial phase velocity at weak optical fields is at $\nu_0 = 0$, the optical wavelength of the output could be noticibly different if the peak gain in strong fields is off resonance. In order to explore this effect numerous simulations like those in the previous sections were performed varying the optical amplitude a_o and the initial phase velocity ν_o.

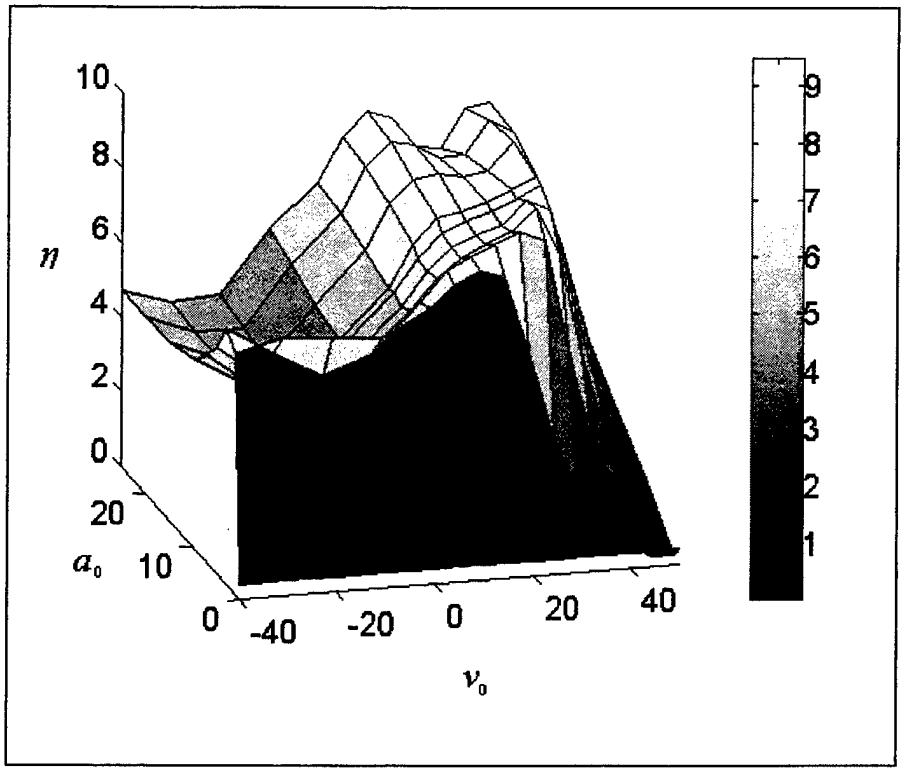

Figure 14. Efficiency versus initial optical amplitude and phase velocity for $\delta = 128\pi$.

Figure 14 shows the results of these simulations for a peak current of 300 A and a taper parameter $\delta = 128\pi$. Constant in all these simulations was the dimensionless current

density $j = 5.5 \times 10^4$, the taper parameter $\delta = 128\pi$, and random Gaussian spread $\sigma_G = 1.3$. The vertical axis is the efficiency, η, and the other axes are the initial optical amplitude, a_0, and the initial phase velocity, ν_0. As the optical amplitude increases, the efficiency peak drifts farther away from resonance culminating in a maximum efficiency of $\eta = 9.3$ % near $a_0 = 20$ and $\nu_0 = 30$, far off resonance. Over multiple passes a_0 will increase and ν_0 will seek the maximum gain, the optical wavelength will change. The expected wavelength shift can be calculated from $\Delta\lambda / \lambda = \Delta\nu / 2\pi N = 30 / 2\pi 100 \approx 5\%$. Over the range simulated in Figure 14, the wavelength could shift by 5 %. This effect could be significant when trying to maximize power delivered through a small atmospheric window.

E. EFFECTS OF PULSE EVOLUTION

When short electron pulses are used they create short optical pulses. Over multiple passes, the arrival of these pulses at the beginning of the undulator must be synchronized. A single-pass simulation is useful in determining the possible short-pulse effects of a design. In order to run the simulations involving pulse evolution, an appropriate filling factor had to be chosen to describe the coupling in the transverse dimensions. Recall that the "filling factor" is the ratio of the area of the electron beam area to the optical beam area, $F = r_b^2 / w_o^2$. The radius of the electron beam is known to be $r_b \approx 0.018$ cm. The radius of the optical mode is less well defined due to the significant diffraction of the optical mode over the last meter of the undulator. Using the 3D simulations involved in the previous sections, it was evident that the optical mode over the untapered section of the undulator was relatively well behaved and could be estimated to

be about $w_0 \approx 0.027$ cm. When the optical mode entered the tapered section, a significant portion of the mode diffracted away from the beam. For simplification a mode radius of $w_0 \approx 0.107$ cm was chosen in the tapered section. This radius included that part of the optical mode having an optical amplitude of at least half of the maximum optical amplitude. Averaging these radii leads to an estimated filling factor of $F \approx 0.07$.

Figure 15 below shows the results of a single-pass through the undulator. The dimensionless current density, j, in this simulation is actually j x F resulting in the value $j = 4000$. The initial phase velocity is $\nu_0 = 0$. The initial optical amplitude was $a_0 = 10$ and the taper parameter matched the RAFEL design at $\delta = 128\pi$ starting at $\tau_s = 0.5$. The electron pulse length is given by $\sigma_z = 3$. The upper-left window shows the optical pulse evolution along the undulator. The vertical axis for all three windows in the middle is dimensionless time evolving from $\tau = 0$ to $\tau = 1$ along the undulator. The horizontal axis represents the calculation window of width W = 6, which is larger than the electron pulse length plus slippage such that the optical pulse fits inside the window. The lower-left window shows the position of the short electron pulse. The light grey color represents the electron pulse at the beginning of the undulator, $\tau = 0$, and the black pulse represents the final position of the pulse after slippage at the end of the undulator, $\tau = 1$. The upper-middle window shows the optical power spectrum development along the undulator. The development of small sidebands in this power spectrum is indicative of the trapped-particle instability. The upper-right window shows the electron phase velocity changes away from $\nu = 0$ along the undulator. The more electrons that are trapped, the larger the peak at $\nu = 0$. The amount the untrapped electrons drift out depends on the taper parameter taper

parameter δ and the field a_0. In this case, the taper starts halfway through the undulator so the untrapped electrons drift out to about $\delta / 2$ or phase velocity of $\nu \approx 200$. The bottom-middle window is a plot of the weak-field gain spectrum for reference. The lower-right window shows the optical power development along the undulator. The final gain for this simulation is $G_f = 4800$ and the efficiency is $\eta = 4.9\%$.

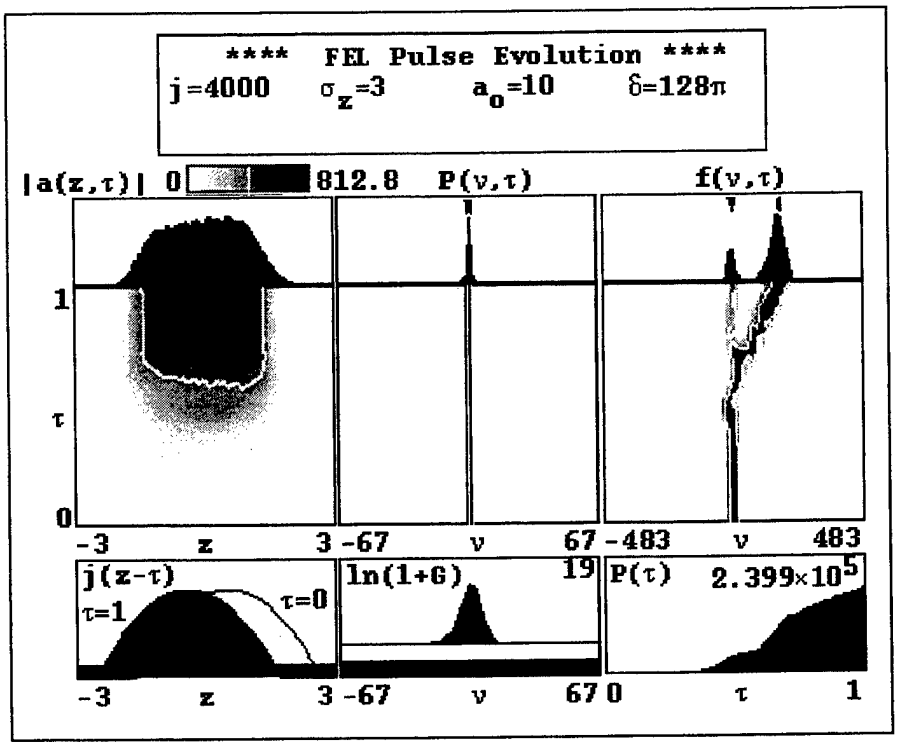

Figure 15. Single-pass pulse evolution simulation.

The parameters in Figure 15 do not result in optimum efficiency. This can be seen by comparing the peaks in the upper-right window. Since about 50 % of the electrons should be trapped for optimum efficiency, the peaks in this window should have roughly equal areas. Too many electrons are untrapped; too few are traped near resonance $\nu = 0$. It is significant to point out that some indication of the trapped-particle instability is

evident even in this single-pass simulation. In order to verify the trapped-particle instability, multiple-pass simulations were performed using the same parameters.

Short-pulse simulations were run over multiple passes using various values of desynchronization. As described previously, the desynchronization value, *d*, represents the timing of the optical feedback pulses relative to the incoming electron pulses. Figures 16, 17, and 18 show the results of the multiple-pass pulse evolution simulations for desynchronizations, $d = 0.1$, $d = 0.15$, and $d = 0.3$ respectively. The feedback in these simulations is $f = 1/(1+G)$ where gain is $G = \left(a_f^2 / a_0^2\right) - 1$, so that the feedback is $f = a_0^2 / a_f^2$. In these simulations, $a_0 = a_f \exp(-1/2Q)$ so $f = \exp(-1/Q)$. The smallest value of feedback at which the FEL would effectively operate was found to be $Q = 0.15$, corresponding to feedback $f = 10^{-3}$. The simulations would not reach saturation at lower feedback values because the taper rate gives low gain in weak fields reducing coupling between the electrons and the optical wave.

The upper-left window represents the optical pulse evolution over *n* passes where black and dark grey indicates higher optical amplitude. The upper-middle window represents the power spectrum evolution over n=100 passes. The upper-right window shows the electron distribution over *n* passes. The lower-left and lower-middle windows are the same as before, while the lower-right window now represents the total pulse power evolution over *n* passes.

Of particular note in these multiple-pass simulations is the power spectrum in the upper-middle window of the simulations. Close examination shows that the peak in the

power drifts off resonance away from $\nu = 0$. This drift was anticipated in earlier simulations in the previous section. The simulations in this section correspond to an initial optical amplitude at the upper limit of Figure 14. The final optical amplitude is approximately $a_f = 700$ leading to $a_0 = a_f \exp(-1/2Q) \approx 25$ for $Q = 0.15$. Measurement of the phase velocity deviation from resonance in Figure 16 showed a change in phase velocity of $\Delta\nu \approx 25$, and a corresponding wavelength variation given by $\Delta\lambda / \lambda = \Delta\nu / 2\pi N = 25 / 2\pi 100 \approx 4\%$. This is in agreement with predictions in the previous section where peaks in the gain spectrum occur off-resonance by $\Delta\nu \approx 25$. The optical power has followed the peaks in the gain spectrum in strong optical fields.

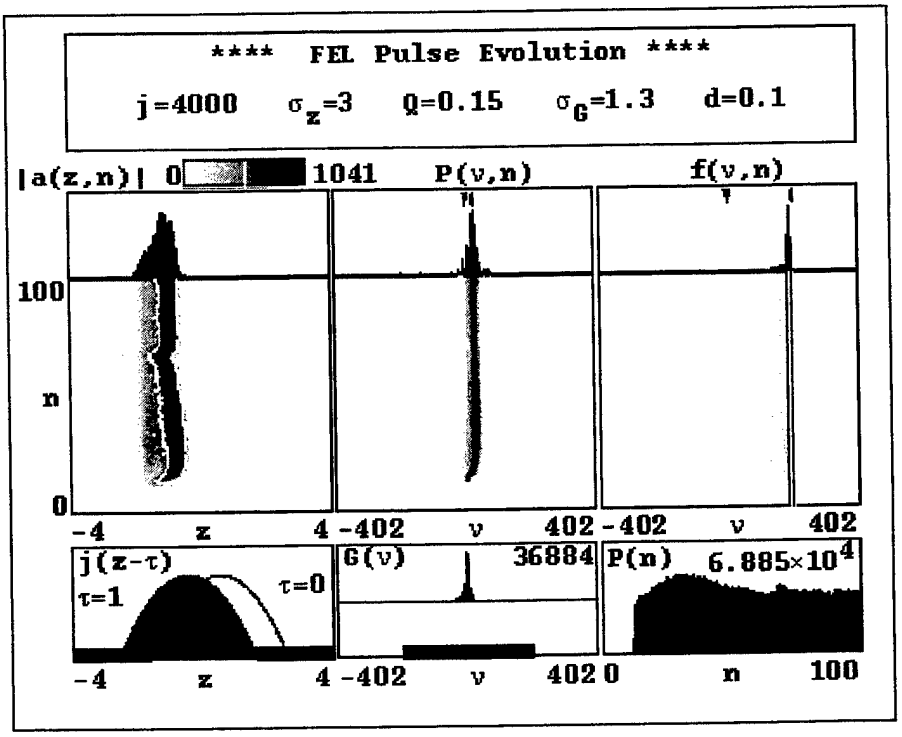

Figure 16. Multiple-pass pulse evolution ($d = 0.1$) simulation.

In Figure 16, the optical pulse is shortener with smaller values of desynchronization [3]. Additionally, the optical pulse is distorted showing the spikes indicating the presence of trapped-particle instability. The power spectrum broadens over multiple passes and the output power fluctuates significantly even after saturation is achieved. The power actually drops off after 30 - 40 passes and then reaches steady state. The final power at $d = 0.1$ is about half the power for optimum desynchronization.

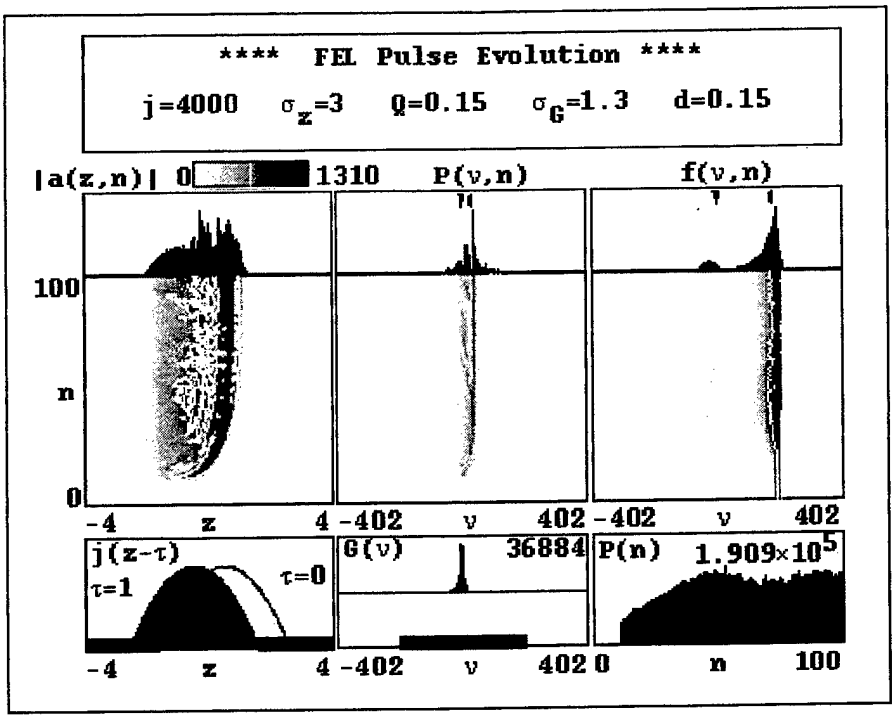

Figure 17. Multiple-pass pulse evolution ($d = 0.15$) simulation.

Figure 17 also shows spikes in the optical pulse and broadening of the power spectrum which indicate the trapped-particle instability. At this intermediate value of desynchronization, the optical pulse is much wider and some electrons still remain trapped.

Figure 18 shows the effects of the trapped-particle instability with a broader power spectrum.

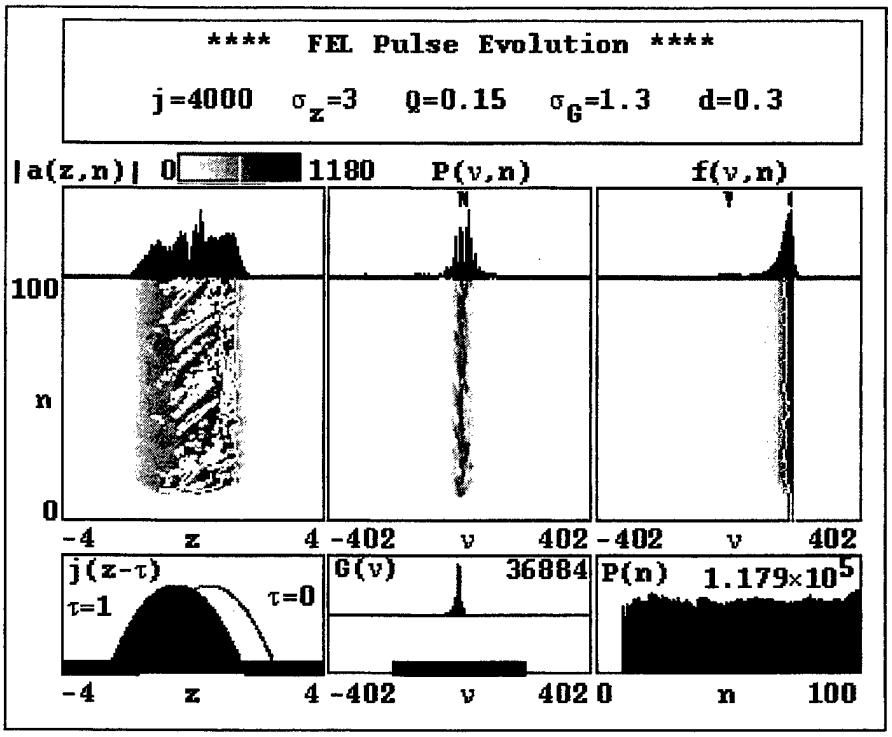

Figure 18. Multiple-pass pulse evolution ($d = 0.3$) simulation.

Figure 19 shows a desynchronization plot for the RAFEL. The plot was compiled using a series of muliple pass pulse evolution simulations using the average power after saturation was reached. The average power was used because power fluctuated by as much as 20% after saturation was reached. The same parameters were used for these results as those for the previous multiple-pass pulse evolution simulations. The x's indicate simulation results and the line traces the estimated curve shape. The o's correspond to the simulations shown in Figures 16, 17, and 18. The trapped-particle instability caused the fluctuations in power over the entire desynchronization range. The

high gain of the RAFEL increases the values of d beyond those associated with traditional FEL oscillators, but the curve shape remains the same.

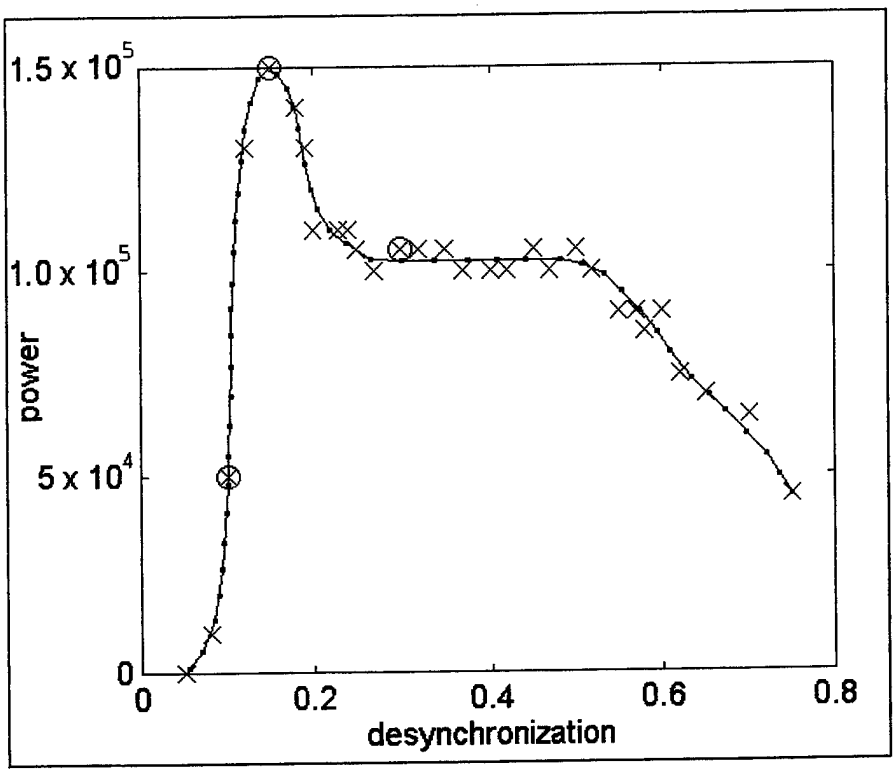

Figure 19. Desynchronization plot for the RAFEL.

F. IDEAL RAFEL OPERATION

In order to get a more complete understanding of the operation of the RAFEL design, one dimensional simulations were run with no diffraction and a perfect electron beam. Figure 20 shows the expected small signal gain spectrum using $a_0 = 1 \times 10^{-6}$ with $j = 4000$ and taper rate $\delta = 128\pi$. The upper window is the gain spectrum for initial phase velocities, $-60 < \nu_0 < 30$. The peak of the gain curve occurs at $\nu_0 \approx 0$ with a

maximum of $G=41{,}280$. The lower window is a plot of the optical phase versus initial phase velocity.

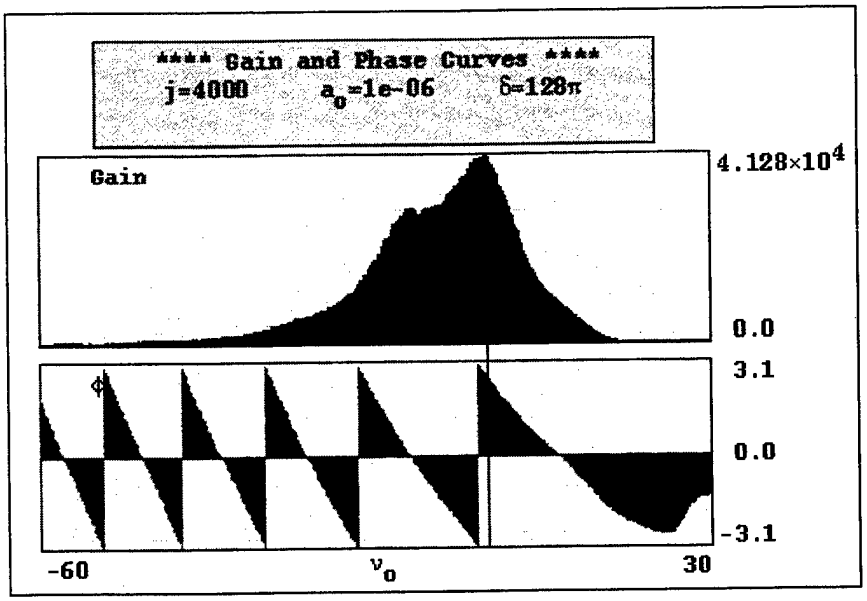

Figure 20. Small signal gain spectrum.

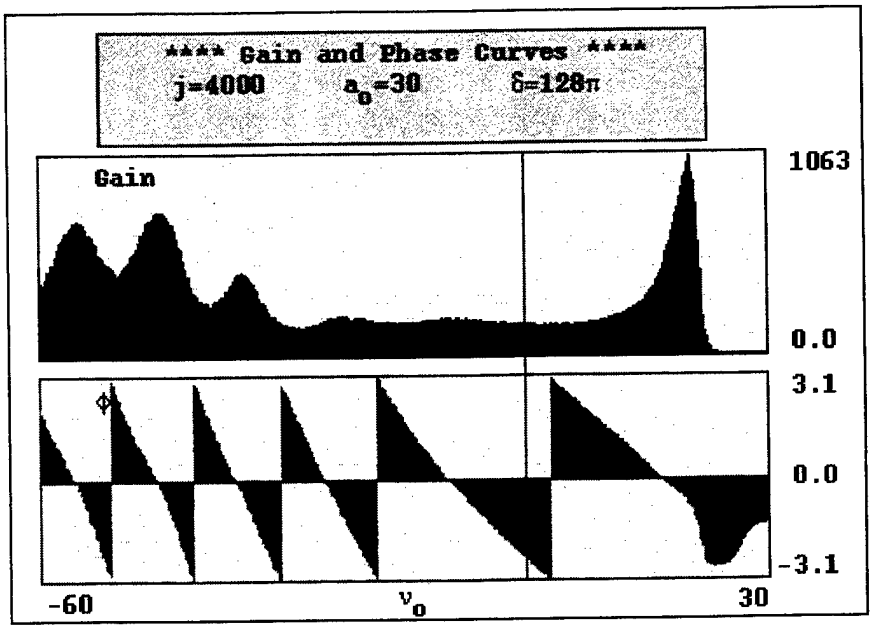

Figure 21. Gain spectrum for $a_0 = 30$.

Figure 21 shows the gain spectrum for $a_0 = 30$ with the same beam and taper parameters as the previous figure. The gain spectrum has a distinctive shape and corresponds to a situation in which a larger amount of optical power has been fed back to the beginning of the undulator. The main peak has shifted to a maximum at $\nu_0 = 20.5$. Recall that Figure 14 showed a peak in the efficiency around this initial phase velocity for $a_0 = 25$. The more dramatic change in the gain spectrum is the development of significant gain peaks for $\nu_0 < -30$. This can be explained using phase space plots.

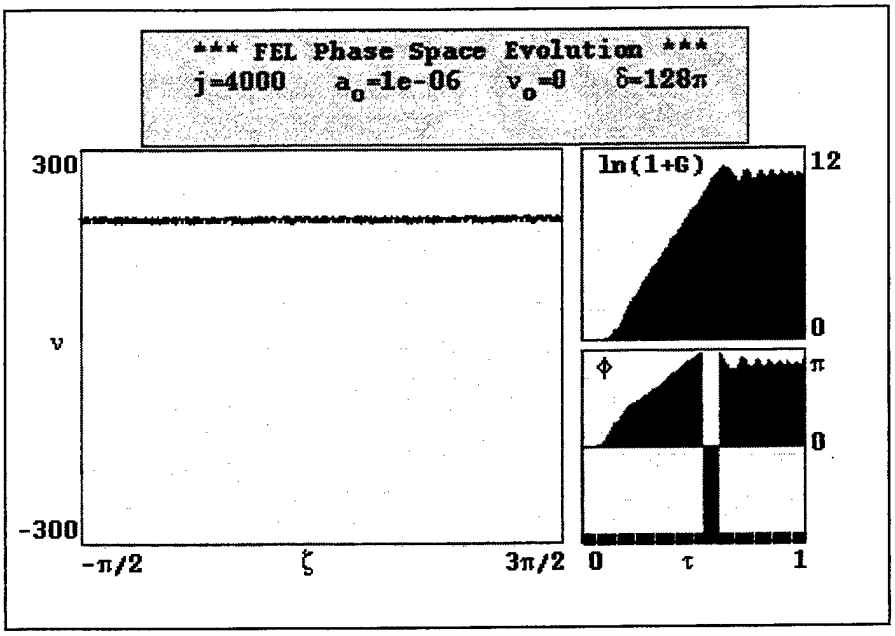

Figure 22. Small signal phase space plot for LANL design.

Phase space plots are useful in understanding the physics behind the gain curve results. Specifically where the electrons are bunching and how many are getting trapped determines the resulting gain. Figure 22 is a phase space plot at $\nu_0 = 0$ using the same parameters as Figure 20. The main window shows the phase space plot with electron

phase velocity along the vertical axis and the electron phase along the horizontal axis. It is evident in the plot that none of the electrons were trapped. This is not surprising since the optical amplitude at $\tau_s = 0.5$ is $a = a_0\sqrt{G} \approx 10^{-4}$ and is not large enough to take advantage of the tapered undulator. The upper-right window shows the natural log of the gain along the undulator. The gain grew significantly during the untapered first half of the undulator, but then leveled out over the last meter where the undulator was tapered but no electrons were trapped. This is indicative of the ineffectiveness of the taper at small initial optical amplitude when there is no trapping. The lower-right window shows the development of the optical phase along the undulator. The phase shift was about π over the first half of the undulator and fluctuated around this value over the remainder of the undulator.

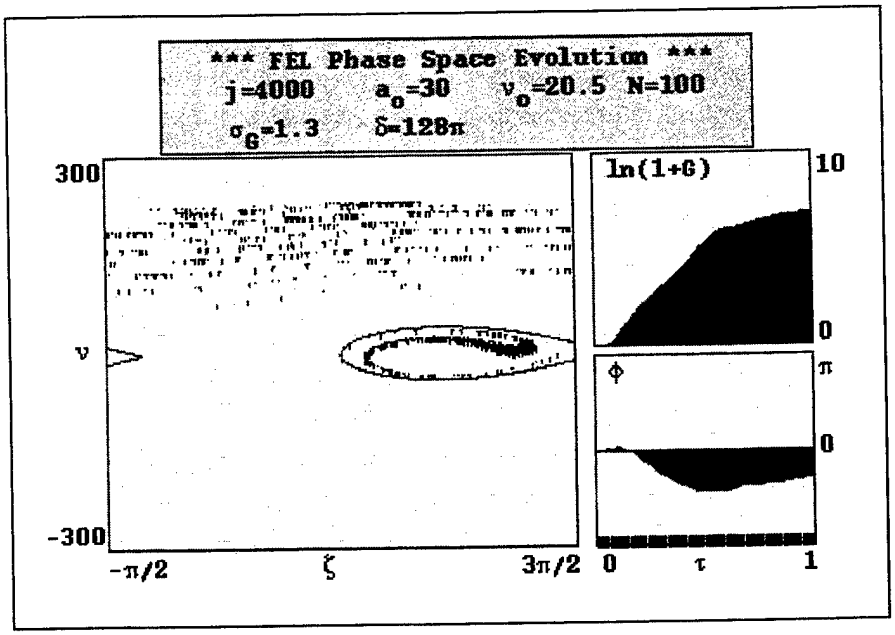

Figure 23. Phase space plot for $a_0 = 30$.

Figure 23 is a phase space simulation at the more optimum value of $\nu_0 = 20.5$ corresponding to the peak in Figure 21. This shows the electron phase development for this optimum condition. About 50% of the electrons are trapped near resonance $\nu = 0$ and bunched around $\zeta = \pi$. The taper works in this case because the field at $\tau_s = 0.5$ is $a = a_0\sqrt{G} \approx 10^3$, and is sufficiently strong to trap electrons. The gain continues to grow throughout the undulator length indicating the taper was effective for this larger optical amplitude.

In Figure 20 the gain spectrum is relatively close to that of an untapered undulator because none of the electrons are trapped. Since the taper is ineffective, the gain spectrum resembles that of an untapered undulator with half the length of the actual undulator. The unique shape of the gain spectrum in Figure 21 is a result of the taper starting point. The peaks in the gain spectrum corresponding to negative initial phase velocities occur because as the electrons increase in phase velocity from the tapers artificial acceleration they become trapped in the separatrix when it is centered near $\zeta + \phi = \pi$ allowing them to contribute to the optical mode. The dips near these peaks correspond to electrons being trapped when the separatrix is not in the optimum area of phase space for gain. The taper should be turned on when the electrons are giving up energy to the optical mode and give an artificial acceleration to keep them giving energy to the optical mode. If the taper is turned on when the electrons are taking energy from the optical mode, it is not as effective or efficient. Also, if the taper amount is too high or too low there will be a change in optical phase and the separatrix will drift across phase space causing the electrons to leak out and diminishing gain.

V. CONCLUSION

The U.S. Navy needs to develop a "speed of light" missile defense capability as an alternative to current technology. The FEL has the potential to provide this capability. The LANL RAFEL design advances research into this capability by combining the oscillator and amplifier FEL characteristics. In order to better understand the characteristics of the RAFEL design, simulations were done addressing feedback and taper optimization, initial phase velocity effects, short-pulse effects, and ideal RAFEL operation.

The taper optimization was performed for peak currents of 300 A and 370 A and a taper starting point halfway through the undulator. In the 300 A case, peak efficiency can be achieved by decreasing the taper rate from the current design of $\delta = 128\pi$ down to $\delta = 112\pi$ or 26% taper instead of 30% taper. For the higher peak current of 370 A, the optimum efficiency occurred at $\delta = 135\pi$. The key to these results is that the higher current led to more effective optical guiding. Higher taper rates cause optical diffraction to overcome optical guiding causing a hole to develop in the center of the optical mode.

The feedback optimization was performed using the designed taper rate of $\delta = 128\pi$ for the same peak currents. This was accomplished by varying the initial optical amplitude corresponding to feedbacks of $f = 10^{-5}$ to 10^{-2}. In the 300 A and 370 A cases, the efficiency was not significantly effected over this range. However, when the initial optical amplitude was reduced further, $a_0 \leq 0.1$, there was no hole in the center and the efficiency dropped dramatically. Additionally, over the entire range of feedbacks the shape

of the optical mode varied. For small feedback there was a significant hole in the center of the optical mode, while at larger feedback there was no hole. Since the feedback amount is dependent on the shape of the optical mode, this introduces another variable in the RAFEL design. Until a steady-state mode of operation is reached, the amount of feedback will vary. A smaller aperture in the downstream mirror would increase feedback and possibly increase efficiency during start up.

The phase velocity giving peak efficiency depends significantly on the initial optical amplitude. Since the RAFEL design involves feedback, the dependence of efficiency on the initial phase velocity could cause a change in the optical wavelength. The wavelength change would be on the order of a few percent, and can be taken into account when designing a RAFEL to operate within a desired wavelength window.

Since the electron beam is really a series of short electron pulses, the effects of short pulses were addressed in simulations. For multiple-pass short-pulse simulations, the RAFEL design would only operate effectively at feedbacks greater than $f = 10^{-3}$. These simulations showed that the optical pulse was significantly distorted by the trapped-particle instability, and the output power fluctuated after reaching saturation.

Simulations indicated that the RAFEL design depends significantly on the taper starting point and taper rate. Since the RAFEL starts from weak fields and tapering is only effective in strong optical fields, it is inherently inefficient at start up. While the gain over the first meter of the undulator is high, it is not high enough to allow efficient use of tapering when the initial optical amplitude is too small. The feedback loop enables the RAFEL design to get through this inefficient phase by seeding the undulator with a small

amount of optical power. The result is a gain spectrum that varies significantly with the initial optical amplitude. As the amount of feedback increases, the fixed taper rate varies in effectiveness. Like the 3D simulations involving initial phase velocity, the ideal simulations showed a shift in the gain peak toward larger values of ν_0 as the initial optical amplitude was increased.

The RAFEL design effectively combines the attributes of the oscillator and amplifier FEL designs. It is inherently inefficient at the beginning of each macropulse when optical amplitudes are small. However, saturation and efficient operation can still be reached due to the combination of high gain and feedback. Detailed experiments, or simulations, should be done on the feedback system to better understand the RAFEL operation, and optical mode development. One of the advantages of the RAFEL design is reduced power on the mirrors. As future designs work toward higher power, better understanding the optical mode development over multiple passes will be important to maintain this advantage. Future work could involve detailed simulation of the feedback loop or design modifications.

LIST OF REFERENCES

[1] M. Wardlaw,"Defense at the Speed of Light", *Surface Warfare*, September/October 1997, Vol. 22, No. 5.

[2] E. J. Anderson, "Total Ship Integration of a Free Electron Laser (FEL)," Master's Thesis, Naval Postgraduate School, September 1996.

[3] W.B. Colson, "Classical Free Electron Laser Theory," *Free Electron Laser Handbook*, W.B. Colson, C. Pellegrini, and A. Renieri (eds.), North-Holland Physics, Elsevier Science Publishing Co. Inc., The Netherlands, 1990.

[4] W.B. Colson, Notes on Derivation of Wave Equation, Naval Postgraduate School, Monterey, CA.

[5] R.L. Sheffield, D.C. Nguyen, J.C. Goldstein, N.A. Ebrahim, C.M. Fortgang, and J.M. Kinross-Wright, "A Compact 1 KW Infrared Regenerative Amplifier FEL", Los Alamos National Laboratory, MS H851, Los Alamos, NM.

[6] W. B. Colson and J. Blau, "Parameterizing Physical Effects in Free Electron Lasers," *Nuclear Instruments and Methods in Physics Research* A272, North-Holland Physics, Elsevier Science Publishing Co. Inc., The Netherlands, 1988.

INITIAL DISTRIBUTION LIST

1. Defense Technical Information Center 2
   8725 John J. Kingman Rd., Ste 0944
   Ft. Belvoir, VA 22060-6218

2. Dudley Knox Library 2
   Naval Postgraduate School
   441 Dyer Rd.
   Monterey, CA 93943-5101

3. Professor William B. Colson, Code PH/Cw 4
   Department of Physics
   Naval Postgraduate School
   Monterey, CA 93943-5117

4. Professor Robert L. Armstead, Code PH/Ar 1
   Department of Physics
   Naval Postgraduate School
   Monterey, CA 93943-5117

5. Lieutenant Mark D. Kesselring, USN 2
   137 Renoir Ct.
   Lake Saint Louis, MO 63367

6. Dr. Richard L. Sheffield 2
   Los Alamos National Lab, MS H851
   Los Alamos, NM 87545

7. John Albertine 1
   109 Kingswood Rd.
   Annapolis, MD 21401

8. Joung R. Cook 1
   Research Physicist, Code 6655
   Naval Research Laboratory
   4555 Overlook Drive, SE
   Washington, DC 20375-5000